THE EFFECTS OF BLUNT LEADING EDGES ON DELTA WINGS AT MACH 5.8

Thesis by

Kenneth F. Nicholson

In Partial Fulfillment of the Requirements

For the Degree of

Aeronautical Engineer

California Institute of Technology

Pasadena, California

1958

ACKNOWLEDGMENTS

The author expresses sincere appreciation to Professor Lester Lees for his discussions and guidance during this investigation. Aid and comments were obtained from Mr. Malcolm Matthews and Dr. Toshi Kubota and are gladly acknowledged. He thanks the members of the Aeronautics Department machine shop for model construction; his wife and members of the GALCIT ten foot wind tunnel for computing, plotting, and sketches; and Mrs. Geraldine Van Gieson for typing the manuscript.

Financial aid during the investigation was deeply appreciated. It was supplied by the Douglas Aircraft Company and the State of California. The investigation was conducted in the GALCIT 5 x 5 inch hypersonic wind tunnel, operated under the sponsorship and with the financial support of the Office, Chief of Ordnance, and the Office of Ordnance Research, U. S. Army, Contract No. DA-04-495-Ord-19.

ABSTRACT

Pressure distributions were measured on a series of four delta wings with subsonic and supersonic leading edges, both sharp and blunt. The blunt leading edge radius was about 0.5 per cent of root chord. Schlieren studies were also made to determine top and side view shock locations. The tests were conducted at a nominal Mach number of 5.8, and at Reynolds numbers between 0.335×10^6 and 0.901×10^6 based on root chord. Angular settings covered a range $-0.2 \leq w/V \leq 0.5$ in pitch at zero yaw (about $-11.5^\circ \leq \alpha \leq +30^\circ$), and a range of $v/V = \pm 0.125$ (about $\pm 7.2^\circ$) at a fixed angle of pitch of 11.5°.

The effects of bluntness were found to be small. Also, the pressures produced by shock wave interactions with the boundary layer, and the inviscid pressures generated by the blunt leading edges, were found to be small compared with the inviscid pressures producing lift on the basic wing. Spanwise pressure distributions show no similarity to those obtained by linearized theory. Centerline lower surface pressure in pitch at zero yaw is bracketed between the Newtonian value $\Delta P/q = 2(w/V)^2$ and the two-dimensional exact value.

TABLE OF CONTENTS

LIST OF FIGURES

Comparison with Other Information

LIST OF SYMBOLS

a	speed of sound
C	$(\mu_e/\mu_w)\,(T_w/T_e)$
d	leading edge diameter or thickness
L	model characteristic length, root chord
M	average free stream Mach number in vicinity of model inside test core
M_n	component of M normal to a leading edge, $M_{no} = M_n$ at $w/V = v/V = 0$
P	measured orifice pressure, referenced to vacuum
P_∞	free stream static pressure in vicinity of model corresponding to M
P_o	reservoir pressure
P_o'	total pressure downstream of normal shock
Pr	Prandtl number
$R_{x'}$, R_L	Reynolds number based on x' or L
S_s, S^s	subsonic, supersonic leading edges as defined by M_{no}
T	temperature
T_o	reservoir temperature
u, v, w	components of $\overline{V}$ along x, y, z axes
u/V, v/V, w/V	direction cosines of $\overline{V}$ along x, y, z; last two used to define model attitude
$\overline{V}$	free stream velocity
x'	boundary layer path length, from edge or stagnation point

α	angle of attack, with respect to plane z = 0
β	angle of sideslip; also $\sqrt{M^2 - 1}$
γ	gas constant; 1.4 for air and 1.67 for helium
$\Delta P/q$	pressure coefficient, $\frac{2}{\gamma M^2}\left(\frac{P}{P_\infty} - 1\right)$
μ	viscosity
ν	kinematic viscosity, μ/ρ
ρ	density
$\bar{\chi}$	$\frac{M^3\sqrt{C}}{R_{x'}}$, interaction parameter evaluated at free stream conditions
$\bar{\chi}_a$	$\bar{\chi}$ evaluated aft of shock

Subscripts

$(\ )_e$	edge of boundary layer
$(\ )_w$	wall (model surface)

I. INTRODUCTION

Approximate solutions to the lifting problem for delta (and arbitrary) wings have been carried out in great detail using linear theory, and these results agree fairly well with the results of force tests at supersonic speeds in the determination of the lift curve slope at zero lift. Jones and Cohen[1] summarize these methods for linear theory, and Lampert[2] has obtained reasonable experimental correlation for the lift curve slope at zero lift for Mach numbers up to 4.6.

The success of linear theory in predicting the lift depends upon a fortuitious cancellation of pressure terms involving α^2 on the upper and lower surfaces. At hypersonic speeds the dominant term on the high pressure side is proportional to α^2, even at moderate α, while the pressures on the "suction side" are limited by vacuum (actually somewhat above vacuum because of viscous effects). Thus linear theory becomes increasingly inaccurate for values of $M\alpha$ above about $\frac{1}{2}$.

Linear theory is also unable to treat blunt supersonic or sharp transonic edges. This problem arises because the actual speed of sound aft of the detached shock ahead of such edges is quite different from the constant free stream value assumed by the theory. For delta wings the shock surface spreads laterally and some lower surface pressure is "lost" because of flow around the edges if the shock surface is detached.

A large body of literature has been accumulating during the last few years concerning the inviscid pressures generated by blunt leading edges in two dimensional flow, and the additional pressures

produced by the local slope of the boundary layer for the case of a sharp leading edge. Because of the strong dependence of the viscous effects on M (usually given as proportional to M^3) it is possible that they could alter the characteristics of delta wings appreciably. These problems, in two dimensional flow, have been approached theoretically by Lees and Probstein, Bertram, Lees, Shen, Li and Nagamatsu, Kuo, Lees and Kubota, and others. An experimental approach was followed by Bertram, Hammitt and Bogdonoff, Bogdonoff and Vas, Kendall, Kubota, Tellep and others. Lees[3] and Bertram[4] summarized the theories for viscous effects with sharp leading edges. Hammitt and Bogdonoff[5] and Lees and Kubota[6] present current theories for the effects of bluntness.

For a truly sharp leading edge ($R_d < 100$) boundary layer build up changes the effective shape of the body thus producing pressures above those for inviscid flow. Weak interaction ($\bar{\chi} < 1$ to 2) requires no pressure gradient correction to the boundary layer growth in a first approximation, but "strong interaction" ($\bar{\chi} > 3$ to 4) includes the relation between boundary layer growth and pressure gradient as an essential feature. Although not mentioned in the literature, viscous induced pressures with sharp leading edges have an obvious upper limit, directly at the edge, of the stagnation value behind a normal shock, because boundary layer growth produces its own "blunt leading edge". For an insulated plate and zero angle of attack, weak interaction theory states that[4]

$$\frac{\Delta P}{q} = 1.2(\gamma-1)\frac{\bar{\chi}}{M^2} + .18(\gamma-1)^2(\gamma+1)\frac{\bar{\chi}^2}{M^2} \quad \text{, (Lees and Probstein)}$$

$$= \frac{.48\, M\sqrt{C}}{\sqrt{R_{x'}}} + .069\, M^4 \frac{C}{R_{x'}} \quad , \quad \gamma = 1.4$$

Strong interaction ($\bar{\chi} >> 1$) for a flat sharp plate with Pr = 1, gives

$$\frac{\Delta P}{q} = .743\frac{\bar{\chi}}{M^2} - \frac{.114}{M^2} \quad \text{, Lees 1st order, } \gamma = 1.4$$

$$= .743\frac{M\sqrt{C}}{\sqrt{R_{x'}}} - \frac{.114}{M^2}$$

Blunt leading edges act like a blast wave in a plane transverse to the flight direction, and near the blunt edge the viscous effects are minor. The relative importance of inviscid (blunt) or viscous (sharp) effects can be estimated in terms of the Reynolds number based on the leading edge thickness. Lees and Kubota[6] have used a blast wave theory and hypersonic similarity to obtain pressures on a blunt (but rounded) plate at $\alpha = 0$. They have also obtained a criterion for the relative importance of viscous and inviscid leading edge effects by comparing the drag produced by each, assuming strong interaction for the viscous effects. Hammitt and Bogdonoff[5] suggest a combination of inviscid and weak viscous effects based on experiments in helium. They used a square-cut blunt edge, and took $C \backsim M^{-.7}$ in estimating R_d for significant viscous effects. For a blunt plate at zero angle of attack,

$$\frac{\Delta P}{q} = .0192\, M\sqrt{\frac{d}{x'}}\left[1 + 40\sqrt{\frac{C}{R_d}}\right] \quad , \quad \gamma = \frac{5}{3}$$

$$= .0192\, M\sqrt{\frac{d}{x'}}\left[1 + \frac{48.5}{\sqrt{R_d}} M^{-.35}\right] ,$$

from which one sees that for equal viscous and inviscid effects $R_d \doteq 400$ at their test Mach number of 13.3. Viscous effects are small for $R_d > 4000$.

The effects of angle of attack on boundary layer induced pressures have been investigated experimentally by Bertram[8] in air at Mach 6.9, by Erickson[11] in helium at Mach 16 - 17, and by Tellep[12] in air at $M \doteq 4$ but at very large $\overline{\chi}$. Erickson's results are somewhat misleading, because he obtained negative values of pressure increments on his wedges for small $\overline{\chi}$, that is, away from the leading edge. In the opinion of the present author this result is caused by the fact that his "two dimensional" wedges are actually low aspect ratio surfaces with large pressure losses at the edges. For large $\overline{\chi}$, his results seem reasonable. Erickson also presents some very good schlieren studies showing the reduction in thickness of the boundary layer as the wedge angle is increased. These photographs, and his pressure measurements near the leading edge, give experimental justification for use of a weak interaction theory with $\overline{\chi}$ evaluated aft of the shock, as indicated by Lees[3].

At hypersonic speeds, pressures on delta wings with blunt and sharp leading edges have been obtained by Bogdonoff and Vas[13, 14] in helium at $M \doteq 13.3$. Their results indicate a non-conical distribution in lift. However, the Princeton helium tunnel (also NACA) has so far been plagued with a strong axial gradient in Mach number, and this gradient produces a first order effect on pressure because of the change in dynamic pressure with M. In particular, $q/P_o \hookrightarrow M^{-\frac{2}{\gamma-1}}$ at large M. In later reports (for example Reference 9) some attempt has been made to correct for this error, but no corrections are

applied in References 13 and 14. In addition to this axial gradient problem, lateral variations in Mach number are always extremely troublesome in any hypersonic tunnel, air or helium, and the calibration is not known for this particular tunnel.

Schlieren studies of Reference 14 show that at very high Mach number and moderate α, the boundary layer is crushed almost flat on the high pressure side of a delta wing even near the vertex, so that viscous induced pressures tend to become small compared to pressures normally associated with lift. Bogdonoff and Vas utilized a set of nearly spanwise orifices near the vertex, which is located at a calibrated point in the tunnel. The data obtained with those orifices (with modest corrections for the gradient of M) will be useful for comparison purposes.

Theoretical approaches for the effects of viscous interaction or the effects of bluntness on delta wings at angles of attack have not been attempted as yet. At the present time there are no theories even for the inviscid pressures, and the viscous contribution is non-linear. Still, some intuitive observations can be made. For example, the pressures at the leading edges must be close to a stagnation value associated with the flow normal to the leading edge, with blunt or sharp edges. Viscous interaction effects along the edges or at the vertex will cancel top and bottom at small α (suggested to the author by Dr. Z. Bleviss). If the streamlines are essentially parallel to the plane of symmetry, some viscous spread of pressure might be expected parallel to an edge, but this effect should be similar to that of a blunt edge, so testing of blunt edges will give some insight to this problem.

At the vertex of highly swept delta wings, boundary layer

induced pressures can be larger than leading edge bluntness effects because M_n is low at small α. In fact, Bertram remarks that bluntness effects $\sim (\cos \Lambda)^{8/3}$ where Λ is the sweep angle. Consequently, a more or less two-dimensional boundary layer growth is found near the vertex. For large α, with low upper surface pressures, or at separation, a strong possibility exists for a nose up moment (pitchup) because of the chordwise distribution of these induced pressures.

In summary, it is clear that more experimental data are needed on delta wings at hypersonic speeds, especially pressure data, and a better understanding of viscous and blunt leading edge effects is also needed. Therefore, the purposes of this experiment are as follows:

1. To study the effects of blunt leading edges on delta wings of reasonable hypersonic geometry.

2. To obtain data at high angles of attack and some sideslip, which might serve as a qualitative basis for an improved delta wing theory.

3. To try to obtain a reasonable comparison with the data of Bogdonoff and Vas[14], in order to evaluate hypersonic boundary layer effects on the characteristics of delta wings.

II. DESCRIPTION OF THE EXPERIMENT

A. Test Environment

Testing was conducted in the GALCIT 5 x 5 inch hypersonic tunnel. Before the test an empty tunnel total head survey was made to determine suitable model locations. These surveys gave contours of stagnation pressure ratios, P_o'/P_o, over several tunnel cross sections. A 13-tube rake was used, with tube spacings of 3/8 inch. Surveys were made for P_o = 88.4, 54.4, 24.4, and 14.4 psi, with $T_o = 255^oF$. The contours for the highest reservoir pressure are shown in Figure 1.

For the two highest reservoir pressures a suitable test region was found between stations 19 and 24 (19 and 24 inches from the throat) with a relatively uniform core of about 2 x 2 inches minimum size at station 24, and with essentially zero pressure gradient. Downstream of station 24 the flow deteriorates rapidly because of the closing of the test rhombus, and various wave interactions. Upstream of station 19 the pressure gradient becomes appreciable and model attitudes would be limited by two intersecting throat waves. The two lowest reservoir pressures are considered unusable for this experiment.

Mach numbers were obtained by averaging the core stagnation pressure ratios, assuming a total head tube recovery factor of 1.0 as indicated by Matthews[15] and using the tables of Reference 16. To provide a Reynolds number variation the pressures chosen were P_o = 88.4 and 44.5 psi. The average core stagnation pressure ratio for the lower test pressure was obtained by fairing the results of the 4 total head surveys.

Model positions were chosen so that the base of the model was at about station 23.5, and the most forward vertex position was at about station 18.75, in order to avoid non-uniform flow regions. In the vicinity of the models, the Mach numbers turned out to be $5.80 \pm .10$ and $5.74 \pm .15$ for P_o = 88.4 and 44.5 psi, respectively. A previous survey had shown the flow angularity in the core to be less than 0.2 degrees (Kendall, GALCIT Internal Memorandum No. 2).

For the models used, the Reynolds numbers are as follows:

Models	P_o, psi	$R_L \times 10^{-6}$
Supersonic Edges	44.5	.335
	88.4	.664
Subsonic Edges	44.5	.454
	88.4	.901

B. Models

Model span was fixed at $1\frac{1}{2}$ inches to avoid intersecting the edge of the core. The models are shown in Figures 2 through 5, and orifice locations are given in Figure 6. To represent the 4 wings (subsonic and supersonic edges, sharp and blunt) 8 models were used to allow forward and aft orifice locations. Models with aft orifices were machined from brass with holes drilled from the base to meet the orifices. Stainless steel tubing was soldered into counterbores at the base.

Models with forward orifices had a brass forward portion,

drilled and counterbored as above, with a Devcon* aft portion cast around the stainless steel tubing. Models with forward orifices and blunt edges were cast entirely in Devcon, with brass tubes spliced to the stainless steel tubes and positioned by a suitable rib, so that the orifices could be drilled into the tubes. Molds for the castings were obtained from the models with aft orifices. Low temperature Devcon was used for molds and castings.

An 80 drill (.0135 inch) was used for the orifices and a 70 drill (.028 inch) was used for the lead holes with a 75 drill necessary near the sharp leading edges. Orifice plugging occurred during the test but was very infrequent. Time lags for readings were about 5 and 10 minutes for the high and low pressures, respectively.

The stings were 3/16 inch drill rod, soldered or cast into the model bases, and tilted downward 1.5 degrees with respect to the plane z = 0. There was about $1\frac{1}{2}$ inches of unsupported length between the model and the support. Steady air loads produced sting deflections of about 2.0 degrees at worst conditions. One case of severe flutter and 2 cases of light flutter occurred but no sting failure resulted. Pressures were unaffected by the light flutter.

C. Equipment

General arrangement of the tunnel setup is shown in Figure 7. Pressure leads were carried rearward inside a tube in passing through the second throat to provide ease of starting and to minimize leaks.

---

* Devcon consists of steel filings mixed with a plastic bonding agent. It is commercially available.

Both a straight and a 15 degree offset support were used to obtain pressure data. These supports are shown in Figures 8 and 9. The actuating rods provided in the tunnel were attached to the supports with pivoting mounts, and pitch was obtained by moving the rods. Design of the supports allowed a point 2 inches ahead of the model base to be kept nearly centered in the tunnel. The models were rolled about the stings for yaw and locked with a simple friction clamp.

For the top view schlierens, supports were 1/4 inch cold rolled steel plate, drilled in appropriate places to attach to the actuating rods for the desired pitch. Again, two supports were necessary to obtain the desired range of pitch. These supports are shown in Figure 10.

A 100 cm. silicone manometer and a mercury manometer were used simultaneously, each with its own vacuum pump. Readings were taken to the nearest millimeter of silicone, with an accuracy of $\pm \frac{1}{2}$ mm. of silicone. The mercury manometer was a standby in case the capacity of the silicone manometer was exceeded. As it turned out, the mercury manometer was not required.

D. Test Procedures

A body axis system of coordinates was used with exact stability equation settings w/V and v/V instead of α and β, thus avoiding useless transformations. These settings also simplify roll sting computations, and allow a simple visual check of the data against Newton's theory. The axis system is shown in Figure 11.

Angle of attack at zero yaw was set with a shadowgraph using the schlieren light, so sting deflections were accounted for. As noted

previously steady air load deflections were about 2.0 degrees at worst conditions (w/V = .5). At w/V = .2, v/V = 0, a deflection of about 1.0 degree was observed. A large portion of this deflection is probably caused by pitching moments of the pressure tubes at this setting. Roll and sting pitch angle were computed assuming this amount of sting deflection. (See Appendix for method.) Roll was set by template and sting pitch angle by calibrated actuating rod readings. The offset support was used for yaw, thus shortening the unsupported length of the actuating rods, and bending of these rods was observed to be negligible.

Three cases of flutter occurred, two of them being light and intermittent. Since the light flutter had no noticeable effect on the trends of the data, it was ignored. However, one severe case of flutter could not be ignored. It occurred with the heaviest model (subsonic blunt, aft orifices). The aerodynamic inputs were probably caused by intermittent upper surface separation near the nose. They were easily detuned from the structural resonance point by pushing the nose of the model slightly through the edge of the core. No noticeable effect was seen on the pressures and since they plotted well with other data, the plots are not marked. All flutter cases occurred at w/V = .5, v/V = 0, P_o = 88.4 psi.

Prior to the test an interesting subject had been raised by Dr. Moller-Christensen concerning the infinite deflections to be expected at the nose of a sharply pointed airfoil with nearly uniform loading. For the models tested, a fairly sharp point was available with the sharp leading edges. The soft brass points would

bend easily if touched, but no noticeable deflections were observed in the tunnel. Dynamic pressure was 1.62 lbs./in.^{2} Assuming an even loading of 1 psi, and "small" deflections, the expression for the deflection shows that the tip would have to be extremely sharp for appreciable bending unless a small ridge angle is used. A low aspect ratio is also assumed

$$L\frac{d^2z}{dx'^2} = -\frac{L \cdot \text{MOMENT}}{E\left(\frac{b h^3}{36}\right)}$$

$$= -\frac{P}{E}\frac{\left(b\frac{x'^2}{6}\right)L}{\frac{b(Ax')^3}{36}}$$

$$= -\left[\frac{P}{E}\frac{6}{A^3}\right]\frac{L}{x'}$$

$$\frac{dz}{dx'} = -\left[\frac{P}{E}\frac{6}{A^3}\right] \ln \frac{x'}{L}$$

$$\equiv 0 \quad \text{at} \quad \frac{x'}{L} = 1$$

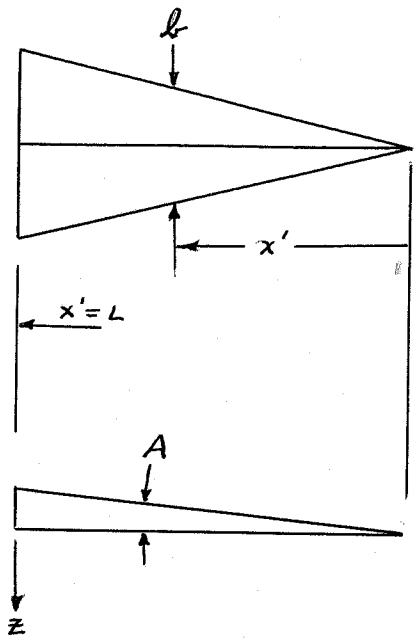

where Ax' = h, depth of triangular section

A = .375/4.75 = .079 for the subsonic sharp model ridge angle

P = 1 psi loading for this calculation

x' = distance from vertex

For $\frac{dz}{dx'} = .01$, $\frac{P}{E} \doteq 10^{-7}$ for brass, $A^3 = 5 \times 10^{-4}$

$$d = A L \left(\frac{x'}{L}\right) = e^{\frac{-(.01)(10^7)}{(1.2\times10^4)}} (.375)$$

$$= e^{-8.33} (.375)$$

$$= 1.3 \times 10^{-4} \text{ inches}$$

It is seen that the ridge angle A plays a very powerful role, that and/large deflections at the vertex would be expected for small A. However, it is impractical to build models or aircraft with the necessary sharpness, or with small depth. Blunt edges as applied in this study stiffened the models considerably.

III. DISCUSSION OF RESULTS

A. Effects of Bluntness

Pressure data for wings with sharp and blunt edges are plotted together to show the effects of bluntness. For a given sweep, at zero yaw, the data are plotted as a function of w/V at constant 2y/b, and as a function of 2y/b at constant w/V. Spanwise data are presented for y positive, using both left and right orifices.

Figures 12, 13, and 14 show the results for the subsonic edges at P_o = 88.4 psi and zero yaw. On the lower surface (Figure 12), the effects of bluntness are rather small, the blunt edges producing slightly higher pressure than the sharp edges at the aft orifices. At the forward orifices, the blunt edge shows a slight increase in pressure at negative w/V, while at the aft orifices both edges are similar. This effect is probably caused by the boundary layer from the upper surface being carried around the edge and supplementing the boundary layer displacement thickness on the lower surface at the forward part of the wing. Sharp edges offer more resistance to this boundary layer flow than blunt edges,particularly near the vertex where the radius of the blunt edge is of the same order as the span.

Vacuum corresponds to $\Delta P/q = -.0425$, and measuring from this level, it is seen that $P/P_\infty \doteq 1.2$ at w/V = 0. The parabolic variation of $\Delta P/q$ with w/V is typical for hypersonic speeds.

The upper surface pressure coefficients lie midway between ambient and vacuum. Separation occurs at a large w/V and it is seen that the blunt edge wing separates first at the forward orifices rather

than at the trailing edge.

Spanwise pressure distributions (Figure 14) are relatively flat. Toward the edge ($2y/b \longrightarrow 1$) pressures rise slightly (high pressure side) at moderate w/V (. 2, . 3) and drop at high w/V as spanwise flow develops. Comparison of the forward and aft data at w/V = . 5 shows a fairly large increase in lift forward that would cause a nose up moment (pitchup). The blunt edges are better in this respect because of the later separation at the trailing edge. This larger pressure forward is believed to be caused by a larger percentage increase in effective span forward than aft as the boundary layer is carried around the edge (suggested to the author by Professor Millikan). Other comments on this effect will be made later in this section.

Figures 15, 16, and 17 show the results for the supersonic edges at P_o = 88. 4 psi and zero yaw. Figure 15 shows the typical parabolic variation with w/V for the lower surface, with the sharp edges now producing slightly higher pressure. The upper surface (Figure 16) pressures indicate that the blunt edge separates forward first as it did for the subsonic edges. Spanwise pressure distributions (Figure 17) show that the pressures rise as $2y/b \longrightarrow 1$ even at large w/V, and spanwise flow is not indicated here. Comparison of forward and aft results at w/V = . 5 shows no pitch-up contribution from the lower surface for either blunt or sharp edges. There is some pitchup contribution from the sharp edge upper surface caused by trailing edge separation. The blunt edge separates forward first, instead of at the trailing edge, thereby producing a nose-down moment.

Results in yaw were obtained only at P_o = 88. 4 psi (Figures 18

and 19). Data were obtained in right and left sideslip, but one set is reversed so that all data are presented for right sideslip. Computed stagnation values are added for the edges to indicate reasonable end points for the fairing. For both subsonic and supersonic edges the effects of bluntness are small. All the rolling moment contribution comes from the lower surface; the contributions from the upper surface are either negligible or opposite in sign. Assuming that the stagnation values are reasonable end points for the fairing, a comparison can be obtained with linear theory. A pressure distribution for linear theory was computed using formula 8, page 158 of Reference 1. It was assumed that both the lower and upper surfaces contributed. With roll referred to body axes, the results are as follows:

	C_ℓ	C_{ℓ_β}	C_{ℓ_β}/C_L
S_s, experimental	-.0049	-.039	-.34
S_s, linear theory	-.0087	-.070	-.52
S^s, experimental	-.0057	-.046	-.34
S^s, linear theory	-.0053	-.042	-.30

Here $C_{\ell_\beta} \equiv C_\ell/(v/V)$ for both linear theory and the experimental values. Since, in linear theory, C_{ℓ_β} evaluated at $\beta \longrightarrow 0$ predicts roll of opposite sign for the supersonic edges, that method was not used.

Data obtained at P_o = 44.5 psi are presented in Figures 20, 21, and 22 for the subsonic edges. Comparison of Figures 14 and 22 shows that the pitchup effect at large w/V found at P_o = 88.4 psi is not present at the lower test pressure. However, except for this item, the

trends are similar. This pitchup will be discussed further in "Viscous Effects".

The results for the supersonic edges at P_o = 44.5 psi are presented in Figures 23, 24, and 25. Comparison of Figures 17 and 25 shows that at large w/V the pressures rise then drop suddenly as $2y/b \longrightarrow 1$ for the lower test pressure. It is thought that the boundary layer builds up in a manner to change the effective shape of the lower surface near the edge. It is also seen that the sharp edge now has a distinct lift advantage in Figure 25. These items will also be discussed in "Viscous Effects".

A difference in P/P_∞ at w/V = 0 is noted between the two reservoir pressures. For example, by comparing Figures 12 and 20, it is seen that at P_o = 44.5 psi, w/V = 0, the aft orifice coefficients are somewhat higher than those at P_o = 88.4 psi. This effect is believed to be caused partly by transmission of pressure from the support forward along the tubes and sting causing the boundary layer to be excessively thick at the trailing edge. Support and tubing interference is also indicated in Figure 24 on the upper surface using the straight support.

B. Schlieren Studies

Typical examples of schlieren photographs are shown in Figures 26 through 33. In Figure 26, subsonic sharp leading edge at w/V = .2, interesting details are the compression waves defining the end of the test rhombus, the crushed boundary layer on the lower surface, and a very thick boundary layer on the upper surface. As evidence that the

upper surface is not separated note the intersection of the upper surface boundary layer with the support; the shock on the support starts at the edge of the boundary layer.

The effects of the presence of the tubes can be seen by comparing Figures 26 and 27, 28, and 29. The start of the shock on the support shows that the upper surface boundary layer is slightly thicker with the tubes than without at w/V = .2 (Figures 26 and 27). There are no noticeable differences on the lower surface. At w/V = .5 (Figures 28 and 29) the only noticeable difference is the presence of a well-defined shear layer, with tubes off, separating the reverse flow from the expanded flow at the trailing edge of the lower surface. In general, the presence of the tubes caused no important changes on the models in any schlieren comparisons.

By looking along the shock surface in Figures 28 and 29, it is seen to be S-shaped. The start of the expansion fan at the trailing edge shows the direction of Mach lines inside the shock surface. Following the Mach lines from the orifice locations shows the slope of the shock surface to be less at points corresponding to the aft orifices than at points corresponding to the forward orifices. Thus the pitchup effect indicated by the pressures at P_o = 88.4 psi is confirmed, but the S-shape of the shock also indicates another region of low pressure between the forward orifices and the vertex. This effect will be discussed under "Viscous Effects". The shock surface for the supersonic edges is straight in this view, and that for the subsonic edges at P_o = 44.5 psi is nearly straight (these are not presented).

The spanwise spread of the shock surface is shown in Figures 30

and 31. A very slight curvature can be seen for the case of subsonic edges. Unfortunately the test rhombus intercepts the shock surface in this case, and the edge of the tunnel window blocks a view of the nose region. So whether or not the top view would show the S-shape characteristic observed in the side view cannot be determined. The shock surface for the supersonic edge is straight from the vertex to a point somewhat aft of the trailing edge, where expansion waves begin to reduce the shock strength. This straight shock surface indicates essentially conical pressure distribution all the way to the vertex.

Figure 31 also shows what is thought to be a free-shear surface between reversed flow and expanded flow leaving the upper surface of the wing. These lines appear on each side of the sting. They appear in the schlierens only when separation is indicated in the pressure data.

Shock surface travel is plotted in Figures 34 and 35. The side view data give a general idea of the amount of pressure relief at the edges as compared to a two dimensional flow. In Figure 34, it is seen that $\frac{d\varepsilon}{d(w/V)}$ is only slightly positive at high pitch, in contrast with the wedge and cone, so that the mass flow must go around the edges. Also ε falls close to the cone value for $.2 < w/V < .4$, and as will be seen later, the pressures are also near the cone value in that range (Comparison with Other Data). Figure 35 shows how the shock moves spanwise to balance the pressures and provides a relief for the mass flow. These top view data indicate one of the problems encountered by linear theory in the hypersonic range.

The exact location of the maximum shock width cannot be determined in these views. Other views, looking along an edge or

looking at a wing rolled at zero yaw would be desirable to complete the shock envelope.

C. Viscous Effects

The experimental data show no large induced pressures associated with two-dimensional boundary layer growth from the vertex or along sharp edges. The schlierens indicate that the boundary layer on the lower surface is crushed flat on the high pressure side at moderate to high α. When the low pressure side is not separated the pressure there tends toward vacuum. As discussed in the introduction, the schlierens of Erickson[11] of wedges at $M \backsim 16.5$ and of Bogdonoff and Vas[14] of a delta wing at $M \backsim 13.3$ also show the boundary layer to be crushed almost flat. This experimental evidence supports the prediction by Lees[3] that the boundary layer effects could be treated by weak interaction for α moderate to large.

Using the method indicated by Lees[3], and taking a slightly different approach using expressions for δ/x and C given by Bertram[4], a limiting form of the viscous pressure coefficient can be obtained for the opposite limiting cases of $\alpha = 0$ and for $M\alpha >> 1$. The details are given in the Appendix.

For $\alpha = 0$ in air, $M >> 1$,

$$(\Delta P/q)_{viscous} \doteq \frac{1.6}{\sqrt{R_L}} \sqrt{\frac{L}{x'}} \sqrt{M} = \frac{1.6}{\sqrt{\frac{\alpha x'}{\nu}}}$$

For $M\alpha >> 1$ in air, an average of two approaches gives

$$(\Delta P/q)_{viscous} \doteq \frac{2.0}{\sqrt{R_L}} \sqrt{\frac{L}{x'}} \sqrt{M} = \frac{2.0}{\sqrt{\frac{\alpha x'}{\nu}}}$$

For $M\alpha >> 1$ in a helium tunnel at "low" temperatures

$$(\Delta P/q)_{viscous} \doteq \frac{1.0}{\sqrt{R_L}}\sqrt{\frac{L}{x'}}\,M^{.65} = \frac{1.0}{\sqrt{\frac{\alpha x'}{\nu}}}\,M^{.15}$$

Written in this form, the induced pressures look much less menacing than they usually appear, and the concept of a hypersonic glide vehicle encased in a boundary layer of extreme thickness does not seem at all probable, at least at moderate to high α. At extreme Mach numbers, $M \backsim 25$ to 30 in air, surface cooling and radiation losses can be counted on to thin the boundary layer further, thus limiting the viscous contribution even more. Skin friction contribution to drag is increased by this process, however.

Assuming $(\Delta P/q)_{viscous} = .05$ at $x'/L = .05$ as a suitable pitchup indication for delta wings caused by essentially two-dimensional boundary layer development near the vertex, then such problems should arise for

$$M/R_L \geqslant (.05)^3/2.0 \doteq .63 \times 10^{-4}, \qquad M\alpha >> 1$$

or

$$L \leq \frac{\nu}{.63 \times 10^{-4}\alpha} \qquad \text{since} \qquad R_L = \frac{a\,M\,L}{\nu} \quad .$$

For an example, at an altitude of 250,000 ft.,

$$L \leq \frac{2.27}{(.63 \times 10^{-4})(1042)} = 34.6 \text{ ft. for mild pitchup from this source at large } \alpha \text{ (neglecting cooling)}$$

A much more severe effect produced by the boundary layer appeared with the subsonic edges. The pressure distributions indicate

spanwise flow around the edges, and the boundary layer is carried around the edge at large pitch. This effect produces a larger percentage span increase forward than aft, and bleeds off some of the boundary layer. The pressure distributions indicate pitchup for P_o = 88.4 psi but not for P_o = 44.5 psi. The side view schlierens (Figures 28 and 29) show an S-shaped shock surface, and this is an interesting point. Both blunt and sharp edges indicate this effect in pressures and schlierens. The S-shaped shock indicates alternating regions of high and low pressure beginning with high pressure at the vertex. This effect does not occur with the supersonic edges where pressures indicate inboard flow from the edge, so it is thought to be caused by boundary layer thickness at the edge, boundary layer bleed, or both, in combination with induced pressure gradients.

For effects of this type, immediate suspicion falls on the lateral tunnel gradients in M, q, or flow angularity, but the gradual buildup of the effect as shown by pressures, and the straight shock front of the supersonic wing rule out these possibilities. Also the variation of the shock location with Reynolds number shows this effect to be caused by viscous action (comparison not presented). Interesting tests to investigate this effect would be as follows:

1. A zero aspect ratio plate at angle of attack (constant span of "infinite" length) to obtain steady oscillations in pressure about the value of stagnation pressure corresponding to the normal Mach number.

2. A long plate of slowly increasing span, to introduce damping.

Another viscous effect appeared with the supersonic edges. The high pressure test resulted in pressure distributions showing a

rising pressure at large w/V for $2y/b \longrightarrow 1$, while those for the low outboard rise and
test pressure show an / then a drop near the edge (Figures 17 and 25). The blunt and sharp edges have about the same level of $\Delta P/q$ at $P_o = 88.4$ psi for the aft orifices, but the sharp edge is definitely higher at $P_o = 44.5$ psi. It is known from the schlieren studies and continuity considerations that mass flow is "lost" around the edges, so the rising pressure distributions must reverse near the edge. It seems probable that the sharp edge resists the boundary layer flow around the edge much more than does the blunt edge. In fact, the constrained region between the shock and the blunt edge might act as a "viscous pump" to bleed the boundary layer continuously from the lower surface of the blunt airfoils.

Thus it is thought that the supersonic sharp airfoils have a maximum boundary layer thickness slightly inboard of the edge in the region of zero spanwise pressure gradient, and the displacement thickness around the edge is relatively large because of slow boundary layer bleed off. With the blunt edges, it is thought that the maximum boundary layer thickness is at the plane of symmetry, and the displacement thickness at the edge is fairly small because of fast bleed off. The larger incremental span effect and the larger average boundary layer thickness could perhaps account for the higher level of $\Delta P/q$ with the sharp edges at $P_o = 44.5$ psi. The maximum displacement thickness slightly inboard of the edges might account for the peculiar spanwise pressure distribution.

Support, sting and tubing effects during the experiment were caused by viscous action. High pressures at the support shock feed

forward through the boundary layer on the tubes and sting, and induce thickening and early separation of the boundary layer on the model. The magnitude of this change in model boundary layer caused by upstream "feeding" from the tubes was shown in the schlierens (Figures 26-29). It is relatively small, but still undesirable since separation angles of attack as indicated by the pressures can be in error. There seems to be no easy way to solve this problem.* The high pressure side should be quite accurate in this respect, however, since no changes are found in the flow due to the tubes.

D. Comparison with Other Information

A summary of the lower surface data, obtained at $P_o = 88.4$ psi with sharp leading edges, is shown in Figures 36 and 37. Various reference levels are added for comparison of pressure distributions. Linear theory pressures are shown for one side only, and the difference between these distributions and experiment is quite large. Adding Newtonian theory to linear theory, on one side only, results in an overestimate of the lift, as expected. Since the upper surface pressures are between $\Delta P/q = 0$ and $-.02$ for these plots, except for separation, $C_L \doteq (\Delta P/q)_{average} + .01$.

Computed stagnation values for flow normal to the leading edge (see appendix) seem to be reasonable end points for the fairing for the subsonic edges, if account is taken of the fact that the pressure falls rapidly away from the edge. However, for the supersonic edges, the

* It might be possible to construct a special schlieren model with thin wire supports in order to observe true separation angles.

stagnation value is low at high w/V. Since the actual location of the shock front near the leading edge is not known, the reason for this discrepancy is uncertain. It is known from the schlieren studies that mass flow is lost around the edges, so a pressure drop toward the stagnation value is necessary as $2y/b \longrightarrow 1$ near the edge.

The limiting form of the pressure coefficient for two dimensional flow $\Delta P/q = (\gamma + 1)(w/V)^2$, fits best for w/V = .3, .4 but is too high at w/V = .5, where mass flow losses around the edges invalidate the approximation. Newtonian theory $\left[\Delta P/q = 2(w/V)^2\right]$ and exact two dimensional theory (i. e., turn along centerline ray), bracket the experimental data everywhere except near the edge at low w/V.

Figure 38 shows a comparison of integrated normal force with various reference values. Some caution in interpretation is necessary here since true integrated forces must be obtained by force tests. Some of the orifices nearest the edge indicate falling pressures as $2y/b \longrightarrow 1$, and the data presented are obtained by estimation in that region. A tangent wedge pressure (exact two dimensional at a local w/V) and a tangent cone pressure (exact cone, at $\alpha = 0$, with a semi-vertex angle equal to the local streamline deflection angle) are applied to one side only for corresponding normal forces. Except for w/V = .5, where the upper surface is separated, the experimental data lie between these two reference values for positive w/V. At negative w/V, the tangent cone approximation matches the data fairly well, but it is noted that no criterion exists as to when to apply the cone, or wedge, or other arbitrary values. As the ridge angle is reduced (i. e., toward a flat plate), these data would tend

more toward values for a tangent wedge. As the wing vertex angle is reduced(toward zero aspect ratio), the result would fall below cone values at high w/V.

Normal force from linear theory (both sides) is plotted so as to pass through the points of zero lift, and shows fair agreement over the range $-.1 < w/V < .2$. However, this agreement is fortuitous, not only because of the cancellation of the terms involving α^2 on a flat non-vanishing plate, but also because of the/ridge angle (or wedge angle for a two dimensional wing). In Figure 38, it is seen that at zero lift C_{N_α} lies / above linear theory for the supersonic edges (ridge angle of 5.46°) is and/about the same as linear theory for the subsonic edges (ridge angle of 4.04°). Decreasing the ridge angle to zero, to obtain a flat plate, would result in C_{N_α} below linear theory at zero lift, as obtained in tests by Lampert[2] at lower Mach numbers. At "infinite" Mach numbers, finite a/ridge angle is necessary to obtain a reasonable C_{N_α} at zero lift, as shown below. Tangent wedge pressures are assumed.

$$C_N = (\Delta P/q)_\ell - (\Delta P/q)_u$$

$$\stackrel{\circ}{=} (\gamma+1)\left[(\alpha+\delta)^2 - (\alpha-\delta)^2\cos^2\eta\right], \quad \delta > \alpha$$

$$C_{N_\alpha} \underset{\alpha \to 0}{\stackrel{\circ}{=}} (\gamma+1)2\delta\left[1+\cos^2\eta\right]$$

where

2δ = angle between ridge and plane $z = 0$

= total wedge angle for two dimensional flow

α' = angle of attack from zero lift

η = wedge angle in plane perpendicular to leading edge for flat bottomed delta wings

Figure 39 shows a comparison between the results of Bogdonoff and Vas[14] in helium (their orifices nearest the vertex) and the present data. The results given in Reference 14 were reduced at the vertex Mach number of 13.3 since the change in $\Delta P/q$ was found to be small if the local value of M was used. Also, these results were extrapolated slightly for $w/V = .2$. This comparison indicates that there are no large changes in the general shape of the spanwise pressure distributions caused by a large increase in $\overline{\chi}$. Differences in the average level of $\Delta P/q$ are attributed to differences in M and γ. It is clear that viscous induced pressures are small for both cases when compared to pressures normally associated with lift.

V. CONCLUSIONS

1. For unyawed delta wings at M = 5.8 with slightly subsonic or slightly supersonic edges, the effects of a leading edge bluntness (1 per cent of root chord) are small. When the wing is yawed so that the advancing leading edge has a normal Mach number of 2.21, the effects of this bluntness are still small.

2. The centerline lower surface pressure in pitch is bracketed between $\Delta P/q = 2(w/V)^2$ and the two-dimensional exact value. For subsonic edges, the pressure near the edge tends toward a stagnation value corresponding to the Mach number normal to the edge. At high pitch angles the pressure falls toward the edge, indicating spanwise flow. For supersonic edges at moderate to low pitch the pressure near the edge rises to a value somewhat above the stagnation value corresponding to the normal Mach number.

3. On the high pressure surface the boundary layer is crushed flat at moderate to large angles of pitch. On the low pressure surface, the boundary layer is quite thick, but trailing edge separation does not occur until the angle of pitch is relatively large. For the delta wing with subsonic edges the boundary layer is carried around the edges, thus creating a relatively larger local span increment, which in turn causes chordwise pressure variations. Controls requirements would appear to be dominated by moments caused by separation at high pitch angles, rather than moments generated by the effects of interaction between shock and boundary layer.

REFERENCES

1. Jones, R. T. and Cohen, D.: High Speed Aerodynamics and Jet Propulsion, Vol. VII, Ch. I, Princeton University Press, Princeton, New Jersey, 1957.

2. Lampert, S.: Normal Force Characteristics of Delta Wings at Supersonic Speeds. Jet Propulsion Laboratory, Report No. EP 236, Revised, February, 1957. Also, Journal of the Aeronautical Sciences, Vol. 24, No. 9, September, 1957, pp. 667-674.

3. Lees, L.: Hypersonic Flow. Institute of the Aeronautical Sciences, Preprint No. 554, June, 1955.

4. Bertram, M. H.: Boundary Layer Displacement Effects in Air at Mach Numbers of 6.8 and 9.6. NACA TN 4133, February, 1958.

5. Hammitt, A. G. and Bogdonoff, S. M.: Hypersonic Studies of the Leading Edge Effect on the Flow over a Flat Plate. Jet Propulsion, Vol. 26, No. 4, April, 1956, pp. 241-246.

6. Lees, L. and Kubota, T.: Inviscid Hypersonic Flow over Blunt-Nosed Slender Bodies. Journal of the Aeronautical Sciences, Vol. 24, No. 3, March, 1957, pp. 195-202.

7. Kendall, J. M., Jr.: An Experimental Investigation of Leading Edge Shock Wave Boundary Layer Interaction at Hypersonic Speeds. Guggenheim Aeroanutical Laboratory, California Institute of Technology, Ph.D. Thesis, 1956. Also, Journal of the Aeronautical Sciences, Vol. 24, No. 1, January, 1957, pp. 47-56.

8. Bertram, M. H.: Viscous and Leading Edge Thickness Effects on the Pressures on the Surface of a Flat Plate in Hypersonic Flow. Journal of the Aeronautical Sciences, Vol. 21, No. 6, June, 1954, pp. 430-431.

9. Vas, I. E.; Bogdonoff, S. M.; Hammitt, A. G.: An Experimental Investigation of the Flow over Simple Two-Dimensional and Axial Symmetric Bodies at Hypersonic Speeds. Jet Propulsion, Vol. 28, No. 2, February, 1958, pp. 97-104.

10. McLellan, C. H.; Bertram, M. H.; Moore, J. A.: An Investigation of Four Wings of Square Planform at a Mach Number of 6.9 in the Longley 11-Inch Hypersonic Tunnel. NACA Report 1310, 1957.

11. Erickson, W. D.: Study of Simple Models at Mach Numbers from 16 to 18 in Helium Flow. NACA TN 4113, October, 1957.

12. Tellep, D. M.: Lift on Flat Plates in Low Density Supersonic Flow. University of California, Report HE-150-131, August, 1955.

13. Bogdonoff, S. M. and Vas , I. E.: An Exploratory Study of a Delta Wing at Hypersonic Speeds. Bell Aircraft Co. Report D 143-978-002, June, 1956.

14. Bogdonoff, S. M. and Vas, I. E.: An Exploratory Study of a Delta Wing at Hypersonic Speeds, Part 3. Bell Aircraft Co. Report D143-978-009, March, 1957.

15. Matthews, M.: Experimental Investigation of Viscous Effects on Static and Impact Pressure Probes in Hypersonic Flow. Guggenheim Aeronautical Laboratory, California Institute of Technology, Aeronautical Engineers Thesis, 1958.

16. Ames Research Staff: Equations, Tables and Charts for Compressible Flow. NACA TR 1135, 1953.

APPENDIX 1

VISCOUS INDUCED PRESSURES

Using the results obtained by Lees[3], and assuming $(\Delta P/q)_{inviscid} = 2\alpha^2$ for a sharply swept delta wing, the variation of viscous induced pressures with M can be obtained by letting C = C(M).

1. From Reference 3, using the notation of that reference, the pressure on a wedge at angle of attack is

$$(P/P_b) = 1 + (2d_b/K^2)\,\bar{\chi}$$

where

d_b = .6(γ - 1) for Pr = 1, insulated plate

P_b = inviscid body pressure

K = Mα >> 1

2. Taking $\sqrt{C} \doteq \frac{2.2}{\sqrt{M}}$ for air, M >> 1

and $(\Delta P/q) = (\Delta P/q)_{inviscid} + (\Delta P/q)_{viscous}$

then $$\frac{\Delta P}{q} = \frac{2}{\gamma M^2}\left[\frac{P}{P_b}\frac{P_b}{P_\infty} - 1\right] = \frac{2}{\gamma M^2}\left(\frac{P_b}{P_\infty} - 1\right) + \frac{2}{\gamma M^2}\frac{P_b}{P_\infty}\left(\frac{2d_b}{K^2}\right)\bar{\chi}$$

$$\left(\frac{\Delta P}{q}\right)_{VISCOUS} = \frac{2}{\gamma M^2}\left(\frac{P_b}{P_\infty}\right)\left(\frac{2d_b}{K^2}\right)\bar{\chi}$$

$$= \frac{2}{\gamma M^2}\left[\frac{\gamma M^2}{2}2\alpha^2 + 1\right]\left[\frac{d_b}{M^2\alpha^2}\right]\frac{M^3\sqrt{C}}{\sqrt{R_{x'}}} \doteq \frac{2d_b M}{\sqrt{R_{x'}}}\frac{2.2}{\sqrt{M}}$$

$$\doteq \frac{2.1\sqrt{M}}{\sqrt{R_{x'}}} = \frac{2.1}{\sqrt{R_L}}\sqrt{\frac{L}{x'}}\sqrt{M}$$

A similar result can also be obtained using the methods listed by Bertram[4].

1. Assuming $(\Delta P/q)_{inviscid} = 2\alpha^2$, and using δ/x aft of shock from Reference 4,

$$\frac{\delta}{x'} = 2.553 \left(\frac{\gamma-1}{2}\right) M^2 \frac{\sqrt{C}}{\sqrt{R_{x'}}} \left(\frac{P}{P_\infty}\right)^{-\frac{1}{2}}$$

$$\frac{d\delta}{dx'} = .255 \frac{\sqrt{C}}{\sqrt{R_{x'}}} \frac{M^2}{\left[1+\gamma\alpha^2 M^2\right]^{\frac{1}{2}}} \quad , \gamma = 1.4$$

2. For C, from Reference 4, $Pr \doteq 1$, where β is the Sutherland constant.

$$C \doteq \left(\frac{\gamma-1}{2}\right)^{\frac{1}{2}} \frac{M\left(1+\frac{\beta}{T_\infty}\right)}{\left(\frac{\gamma-1}{2}\right)M^2 + \frac{\beta}{T_\infty}} \quad , \quad M >> 1$$

$$\doteq \frac{2}{\left(\frac{\gamma-1}{2}\right)^{\frac{1}{2}} M} \quad \text{for } \beta/T_\infty \hookrightarrow 1$$

$$\doteq \frac{4.5}{M} \quad , \gamma = 1.4$$

$$\frac{d\delta}{dx'} \doteq \frac{.54}{\sqrt{R_L}} \sqrt{\frac{L}{x'}} \frac{M^{3/2}}{\left[1+\gamma\alpha^2 M^2\right]^{\frac{1}{2}}}$$

$$\doteq \frac{1}{\alpha} \frac{.46}{\sqrt{R_L}} \sqrt{\frac{L}{x'}} \sqrt{M} \quad , \gamma M^2 \alpha^2 >> 1$$

3. With $\Delta P/q = 2\left[\alpha + \frac{d\delta}{dx'}\right]^2$, $\frac{d\delta}{dx'} << \alpha$, $\gamma M^2\alpha^2 >> 1$

$$(\Delta P/q)_{viscous} \overset{\circ}{=} 4\alpha\frac{d\delta}{dx'} \overset{\circ}{=} \frac{1.84}{\sqrt{R_L}}\sqrt{\frac{L}{x'}}\sqrt{M}$$

Using strong interaction theory, and accounting for the variation of C with M, induced effects can also be estimated for $\alpha = 0$. Here it is assumed that the effects are essentially two-dimensional.

1. From Section I, for air

$$(\Delta P/q) = \frac{.743\ M\sqrt{C}}{\sqrt{R_{x'}}} - \frac{.114}{M^2}$$

$$= \frac{1.63}{\sqrt{R_L}}\sqrt{\frac{L}{x'}}\sqrt{M}\ ,\ M >> 1\ ,\ \sqrt{C} \overset{\circ}{=} \frac{2.2}{\sqrt{M}}$$

It is also of interest to estimate these effects for helium. Here a power law is more suitable for viscosity since high temperatures are not used in the helium tunnels. Use of high temperature would make $(\Delta P/q)_{viscous} \backsim M^{.5}$.

1. $C = \left(\frac{\gamma - 1}{2}\right)^{\omega-1} M^{2(\omega-1)}\ ,\ M >> 1$

$$= 1.467\ M^{-.7},\ \gamma = 1.67,\ \omega = .65$$

2. Using the results of Reference 3, $d_b = .6(.67) \overset{\circ}{=} .4$, $Pr = 1$, for an insulated plate at angle of attack

$$(\Delta P/q)_{viscous} \overset{\circ}{=} \frac{2\,d_b\,M}{\sqrt{R_{x'}}}\sqrt{C}$$

$$= \frac{.97}{\sqrt{R_L}}\sqrt{\frac{L}{x'}}\,M^{.65}$$

APPENDIX 2

SETTINGS IN YAW

If it is assumed that only sting deflections caused by normal force and pitching moment are large enough to have an effect, then settings for yaw can be obtained as follows:

To obtain φ, η : given w/V, v/V, δ

$$(\sin\eta\cos\varphi)\cos\delta + (\cos\eta)\sin\delta = w/V$$

$$(\sin\eta\cos\varphi)\sin\delta - (\cos\eta)\cos\delta = -u/V$$

$$= -\sqrt{1 - (w/V)^2 - (v/V)^2}$$

$$\text{then } \cot\varphi = \frac{\sin\eta\cos\varphi}{(v/V)}$$

$$\sin\eta = \frac{\sin\eta\cos\varphi}{\cos\varphi}$$

where

φ = roll angle about undeflected sting axis

η = undeflected sting pitch angle, with respect to free stream

δ = angle between plane z = 0 and support end of sting, including deflections

APPENDIX 3

COMPUTED PRESSURES

Stagnation values are obtained by assuming that flow normal to a leading edge crosses a normal shock, and that flow parallel to the edge contributes nothing to the pressure. Actually the shock surface is not parallel to the edge in general, but the error introduced is small for small angular errors up to 5 degrees. The true stagnation pressure would be higher than the values assumed, but no reliable method is known for positioning the shock surface.

The stagnation pressure is given by the expression

$$\Delta P/q = \frac{2}{\gamma M^2} \left(P_o'/P_o - 1 \right)$$

where P_o'/P_o is the value corresponding to $M = M_n$ (Reference 16),

and $$M_n^2 = M^2 \left\{ (u/V \sin \tau_o + w/V \cos \tau_o)^2 + (w/V)^2 \right\}$$

For two dimensional or conical flow deflections $\Delta P/q$ is obtained from Reference 16 for a wedge or cone semi-vertex angle, θ, at $M = 5.8$, where

$$\cos \theta = \left\{ u/V \cos \tau_o - v/V \sin \tau \right\}, \quad \tau = \tau_o \text{ at edge} .$$

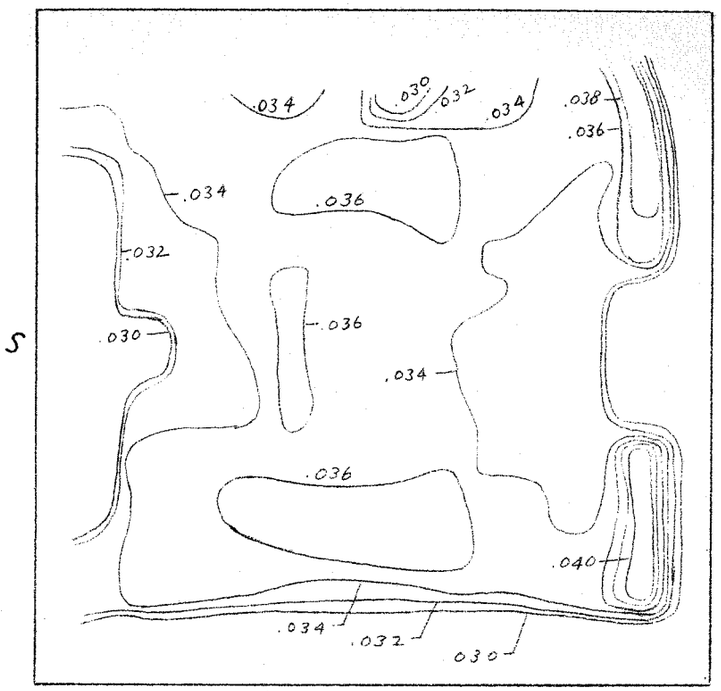

STA. 19

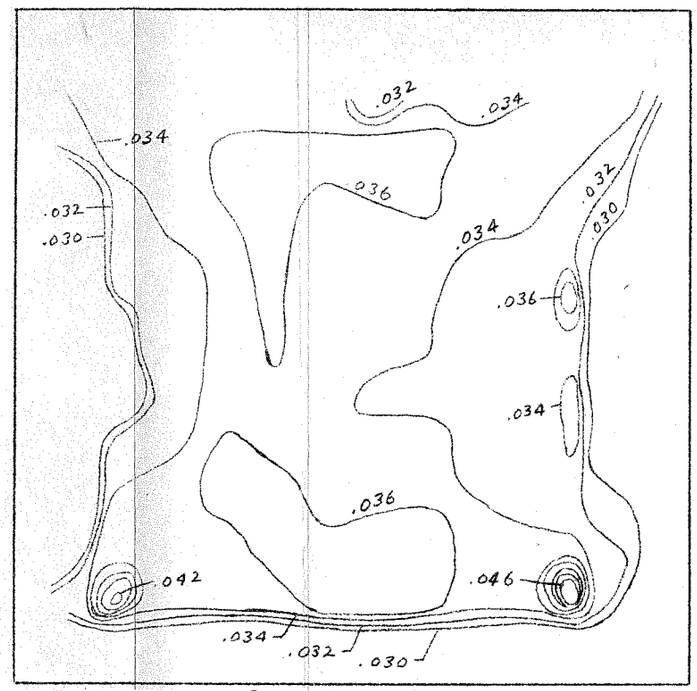

STA. 20

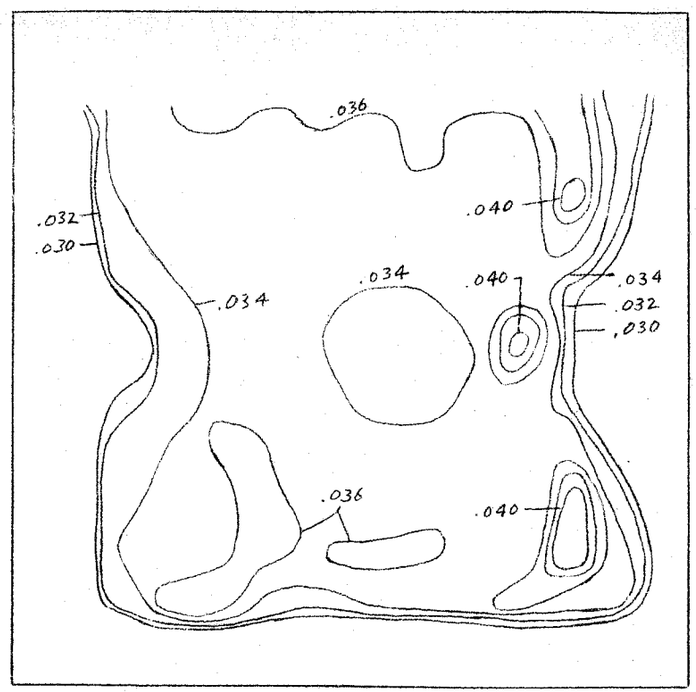

STA. 21

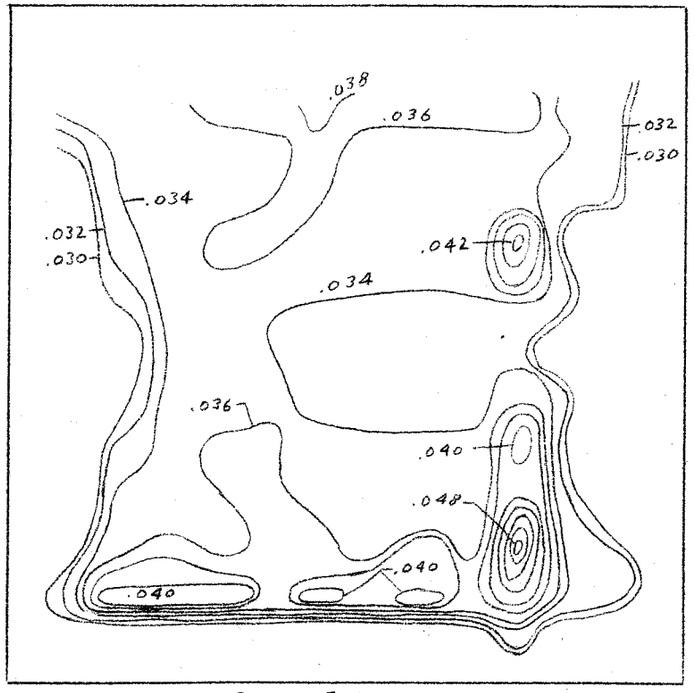

STA. 22

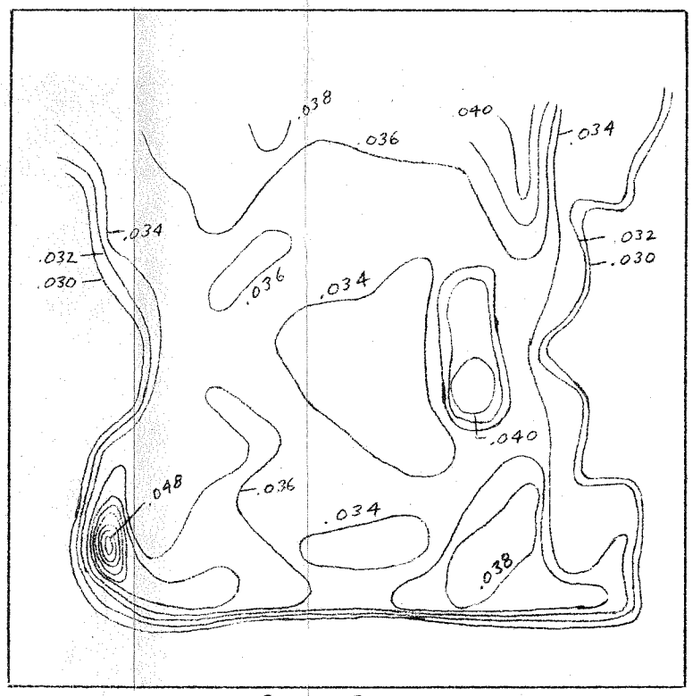

STA. 23

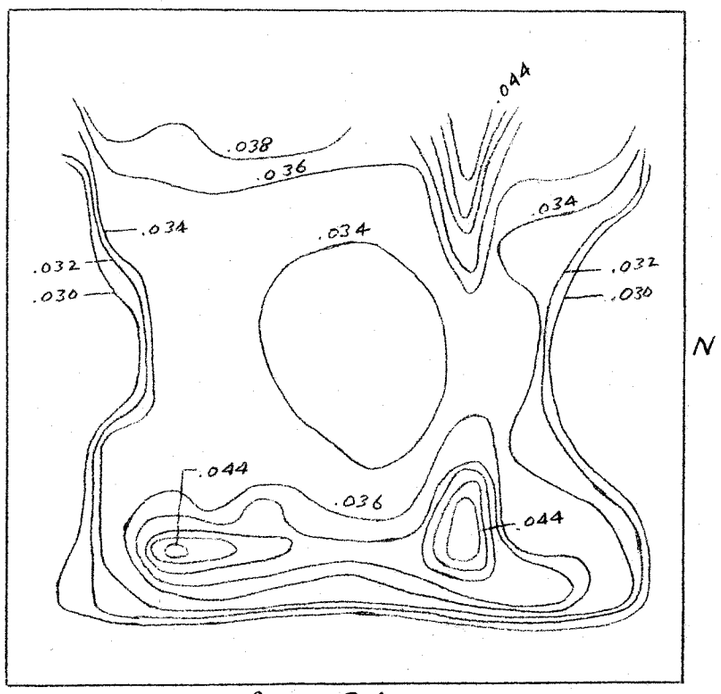

STA. 24

FIG. 1 TUNNEL FLOW SURVEY, $P_o = 88.4$ PSI, CONTOURS OF P_o'/P_o

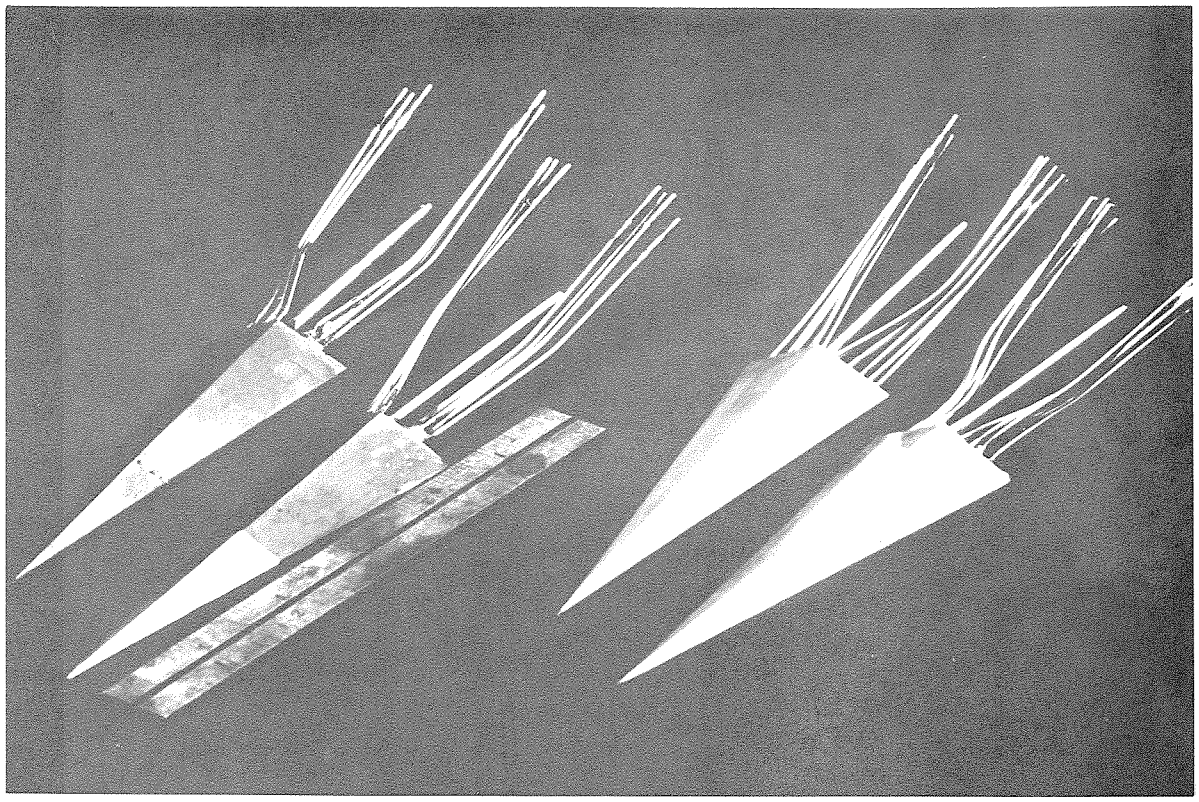

Fig. 2 Models with subsonic edges

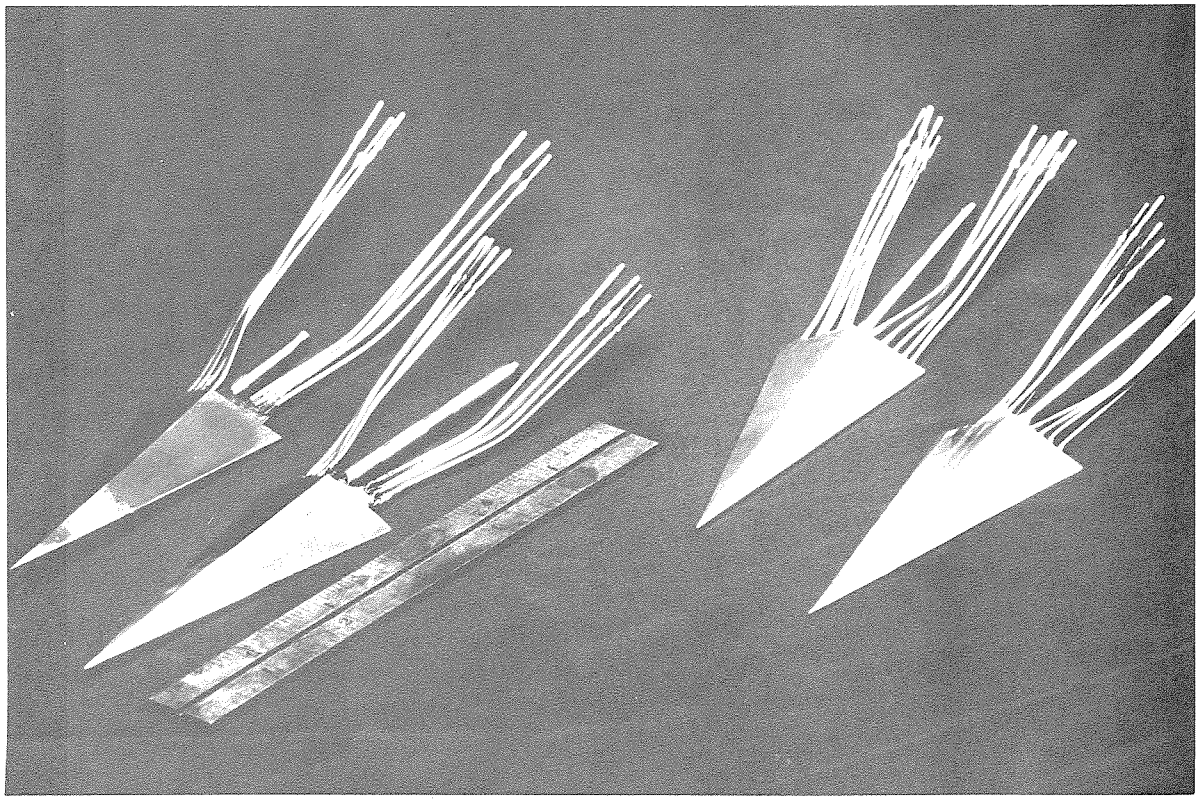

Fig. 3 Models with supersonic edges

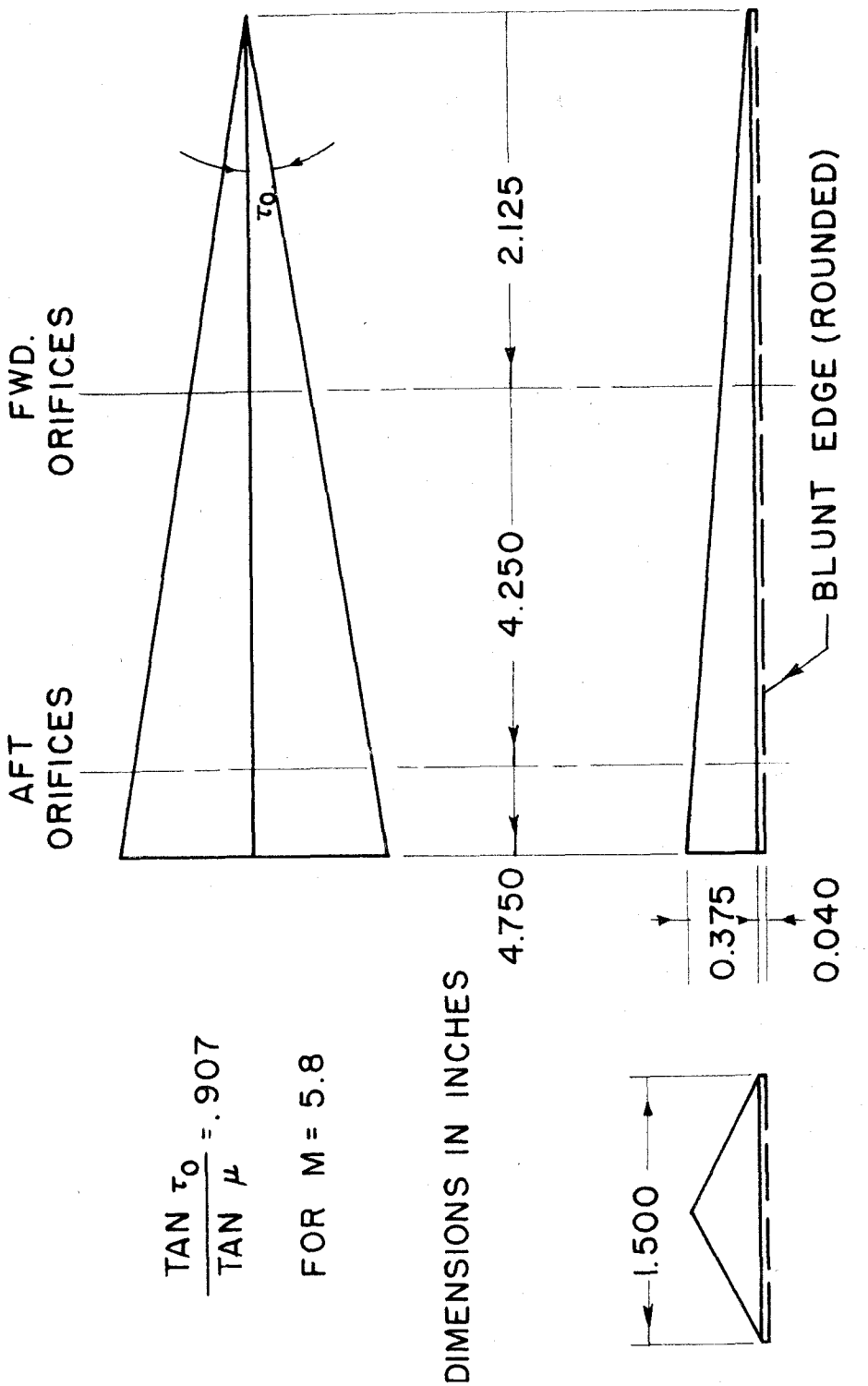

FIG. 4 SKETCH OF MODELS WITH SUBSONIC EDGES

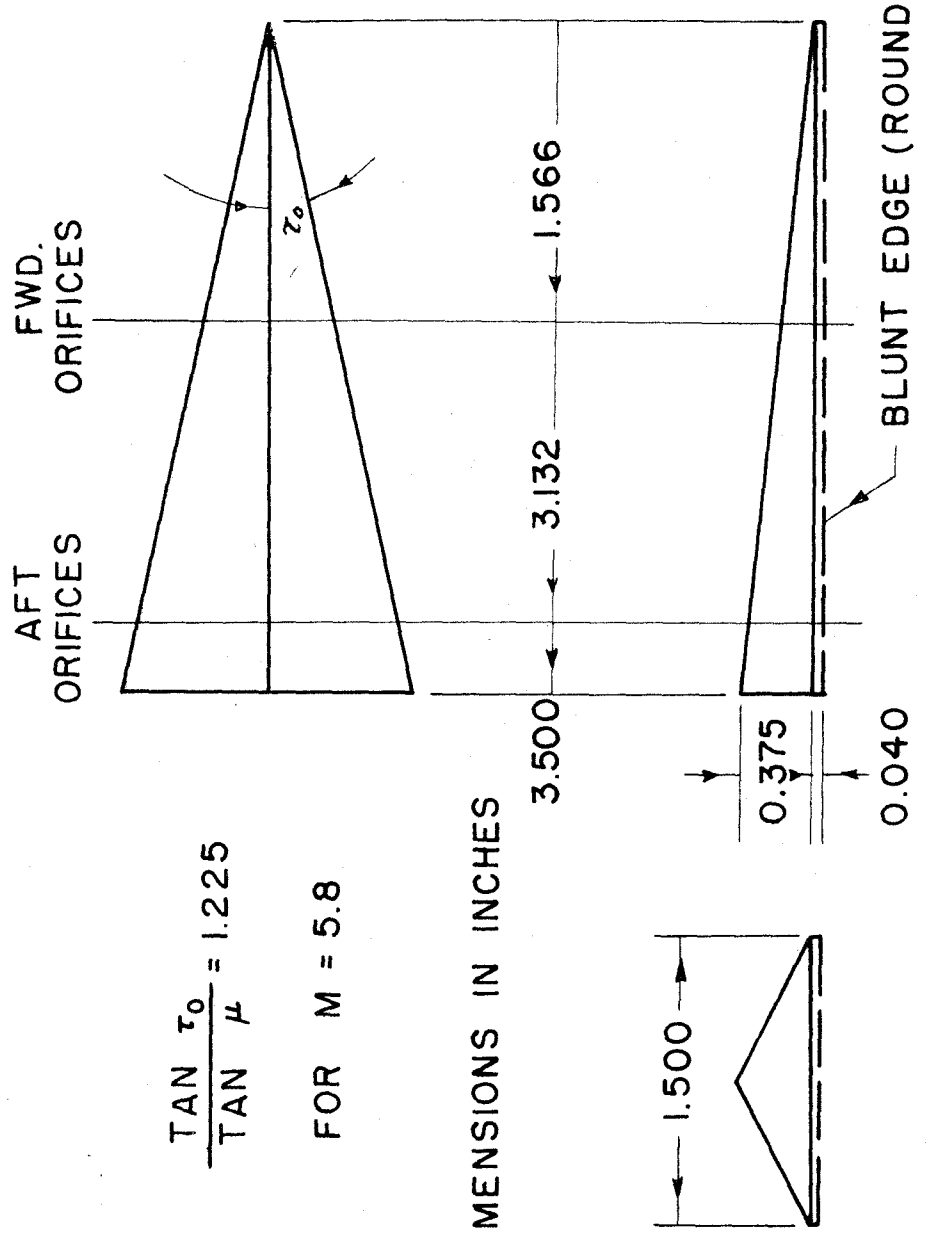

FIG. 5 SKETCH OF MODELS WITH SUPERSONIC EDGES

ORIF.	2y/b
1	-.75
2	-.43
3	-.11
4	.27
5	.59
6	.88
7	-.88
8	-.59
9	-.27
10	.11
11	.43
12	.75
13	-.55
14	-.13
15	.34
16	.76
17	-.76
18	-.34
19	.13
20	.55

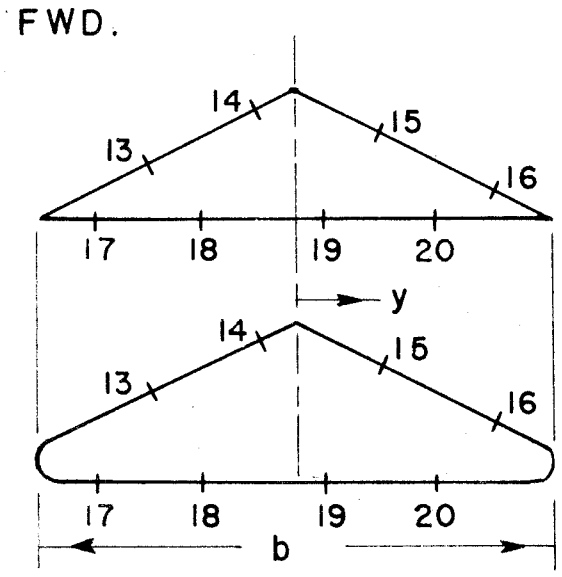

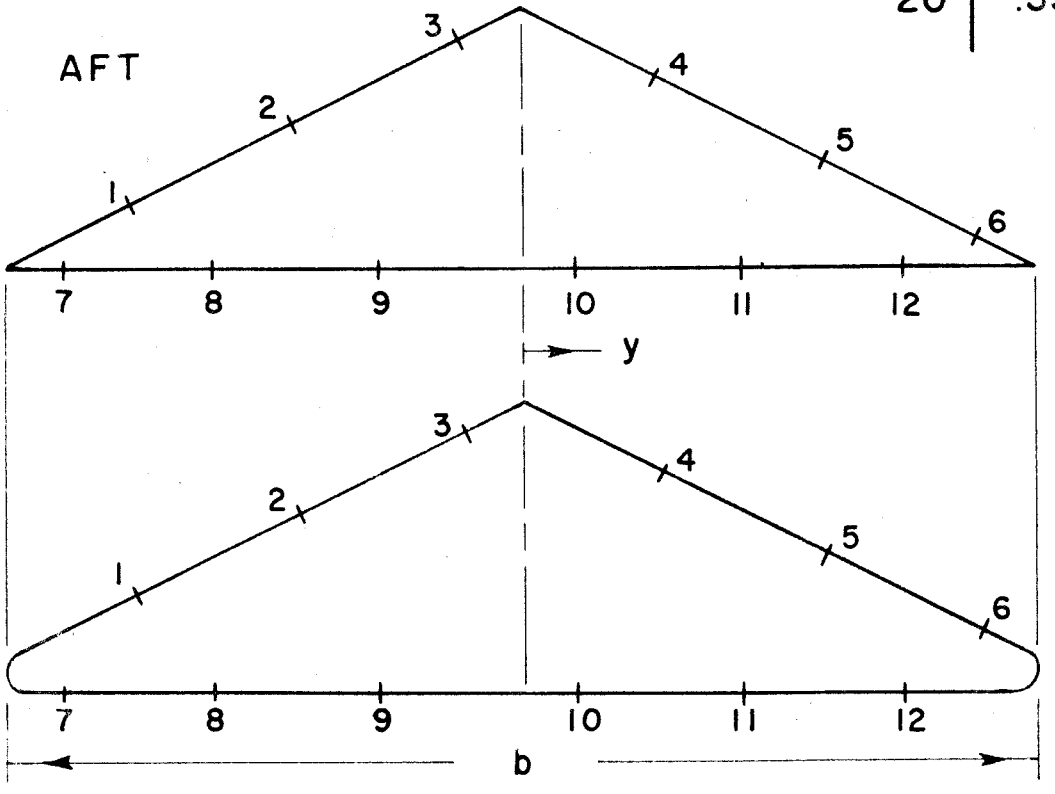

FIG. 6 ORIFICE LOCATIONS

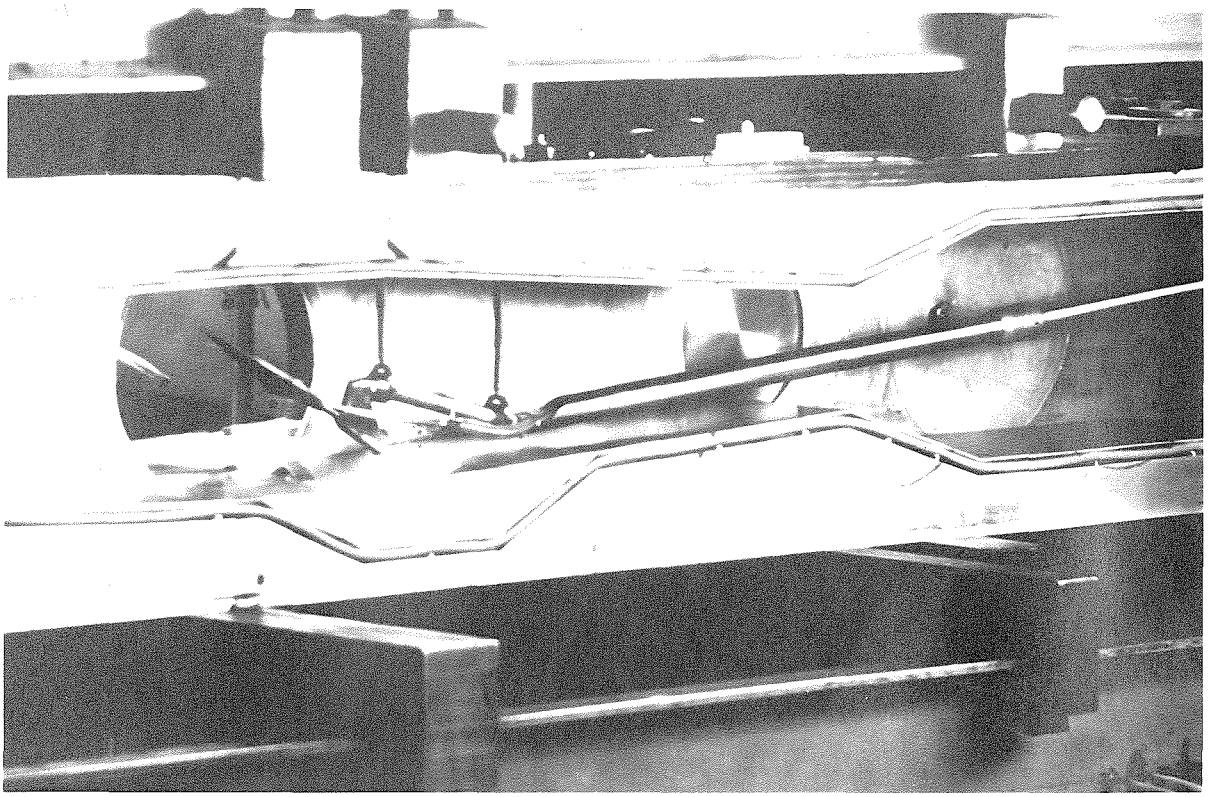

Fig. 7 Duvel set up

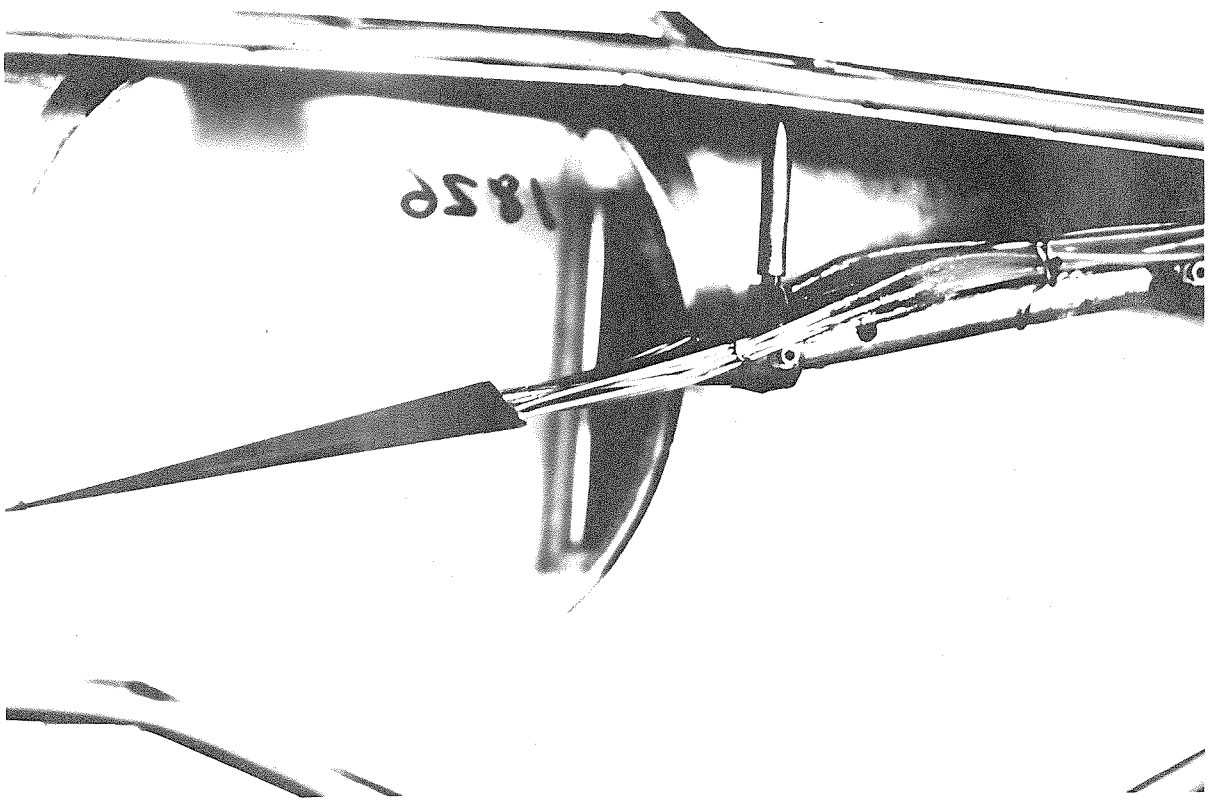

Fig. 8

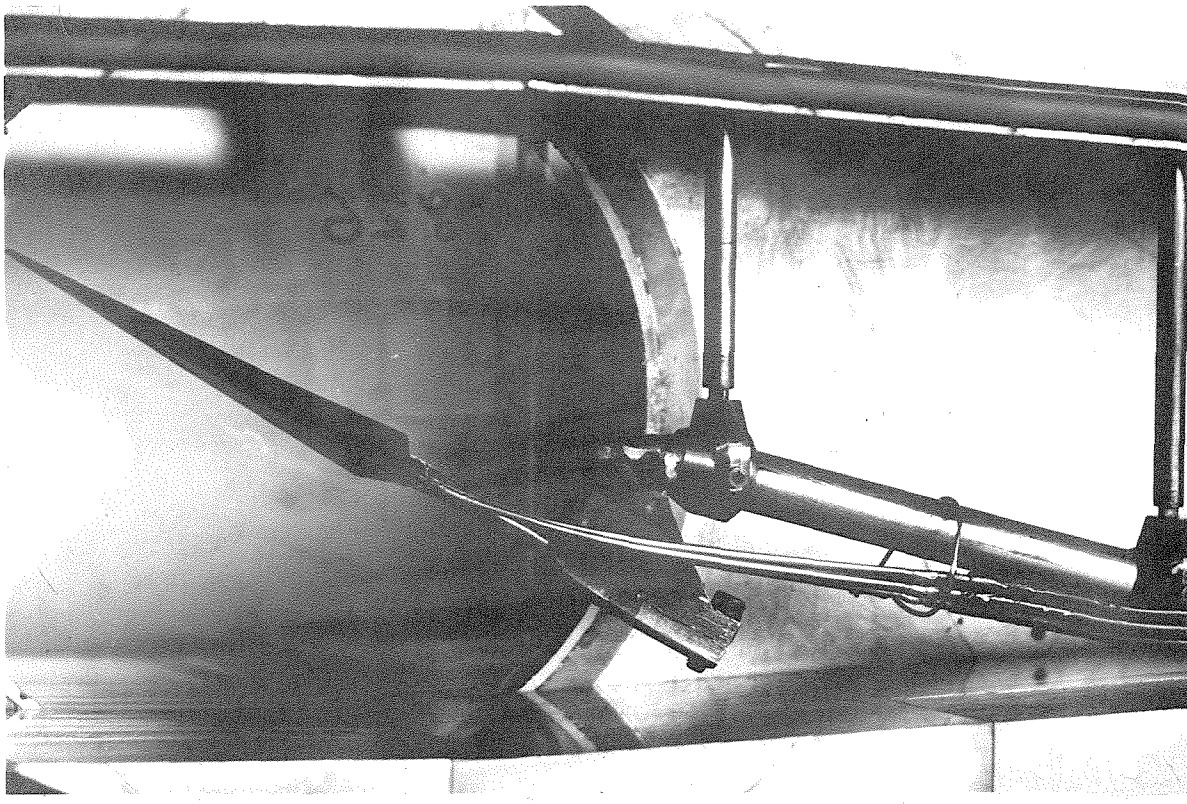

Fig. 9 High w/V with offset support

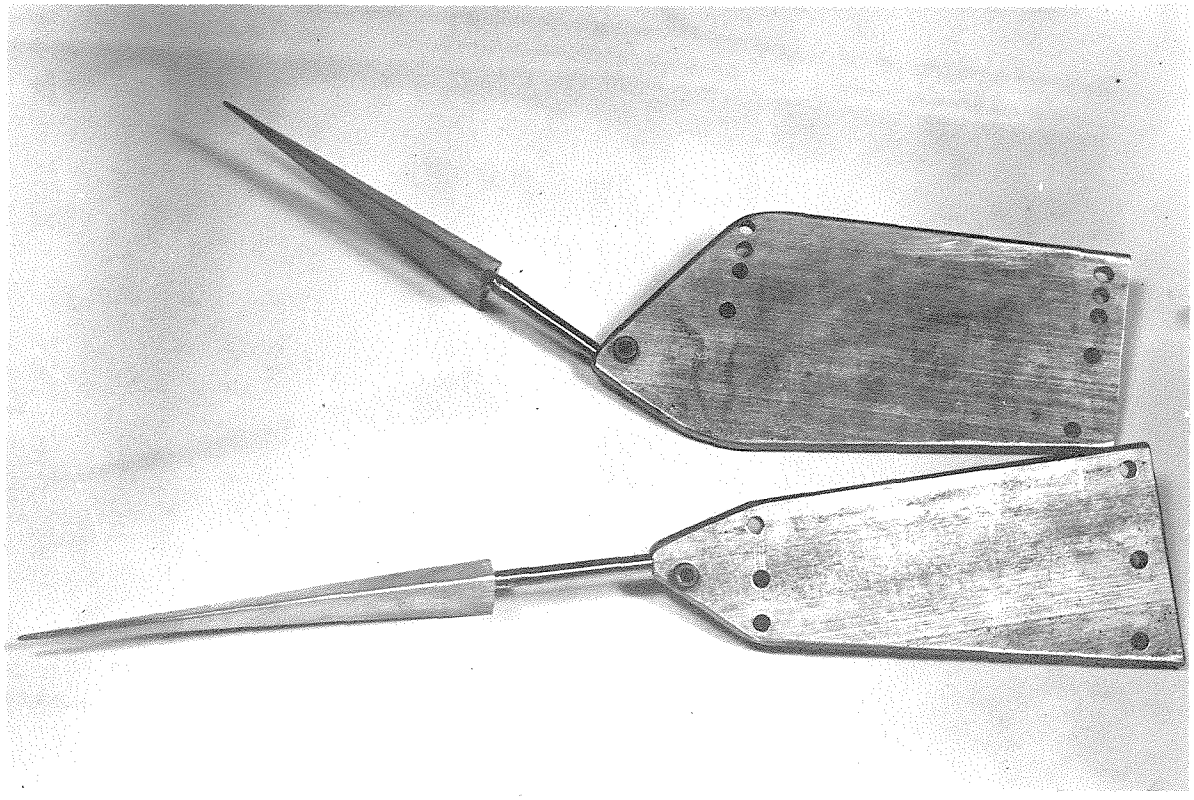

Fig. 10 Setup for top view Schlierens

NOTE: (1) LOWER SURFACE IN X–Y PLANE

(2) $\bar{V}$ = VEHICLE VELOCITY IN STILL AIR
$= u\bar{i} + v\bar{j} + w\bar{k}$

(3) α SET AT $\beta = 0$
β SET AT CONSTANT α

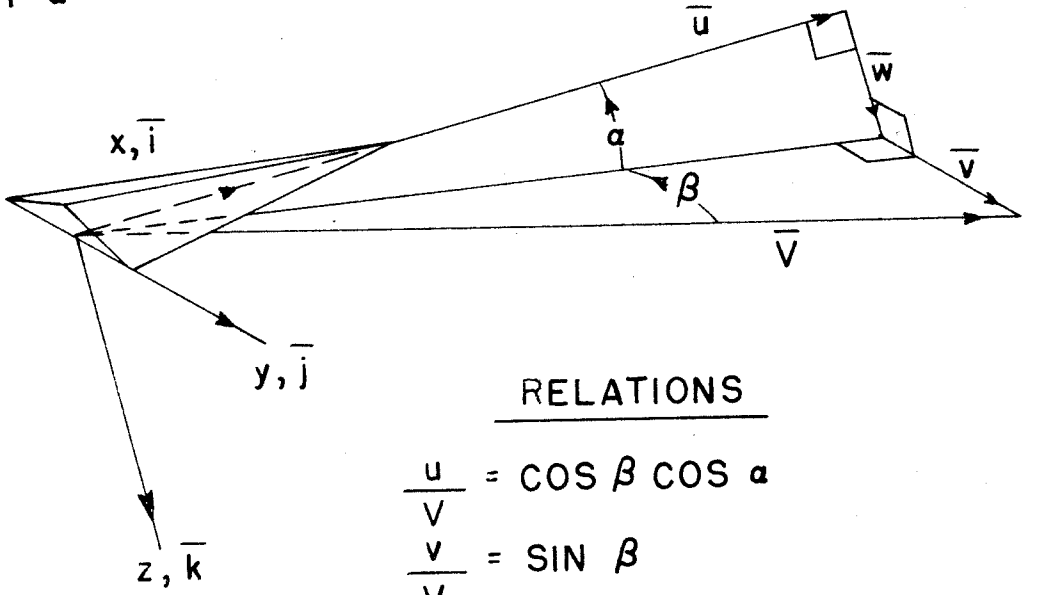

RELATIONS

$$\frac{u}{V} = \cos\beta \cos\alpha$$

$$\frac{v}{V} = \sin\beta$$

$$\frac{w}{V} = \cos\beta \sin\alpha$$

FIG. 11 BODY AXIS SYSTEM

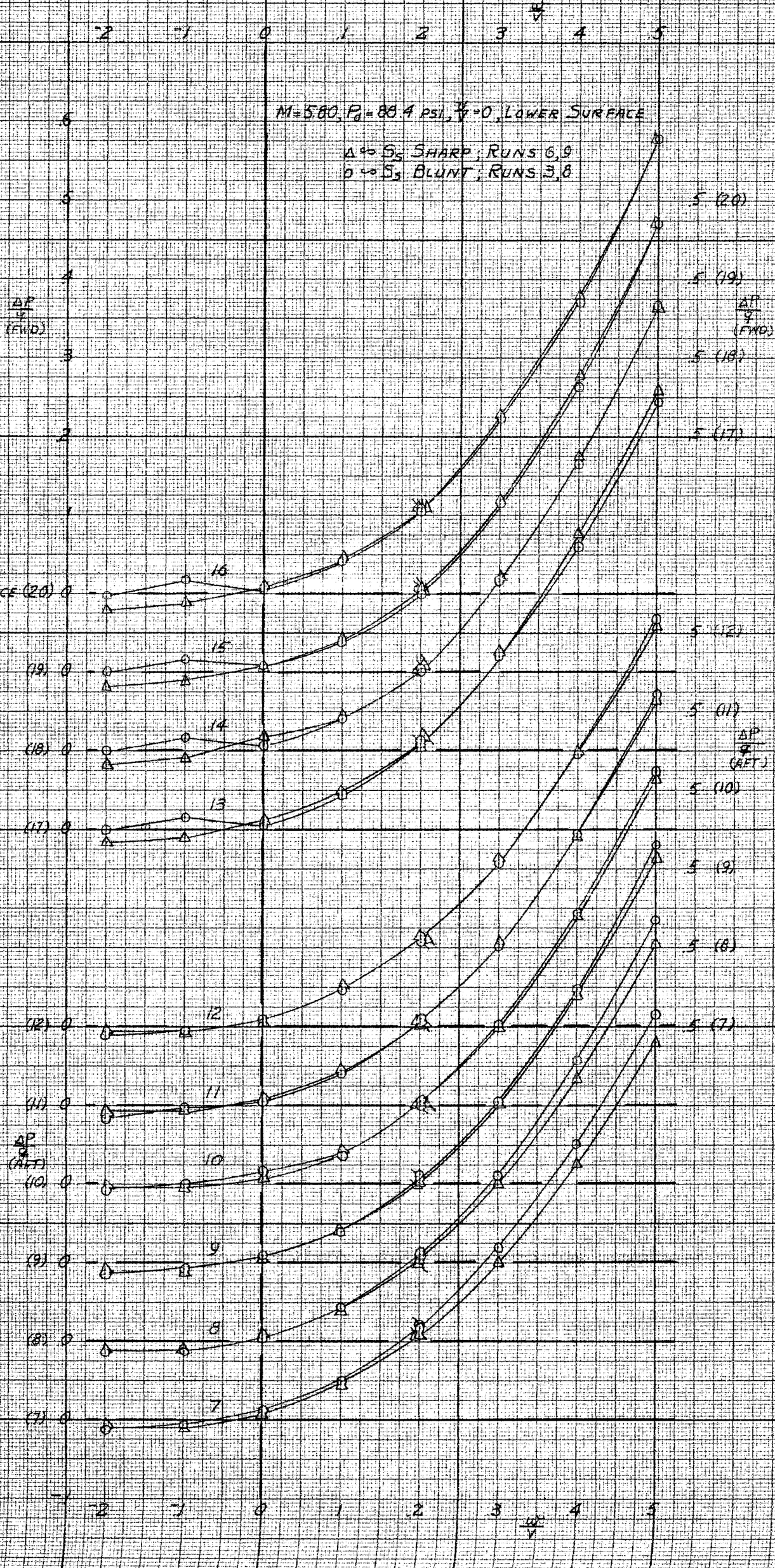

FIG. 12 EFFECTS OF BLUNTNESS, SUBSONIC EDGES, LOWER SURFACE, P_d=88.4 PSI, $\frac{\Delta P}{q}$ VS $\frac{x}{y}$

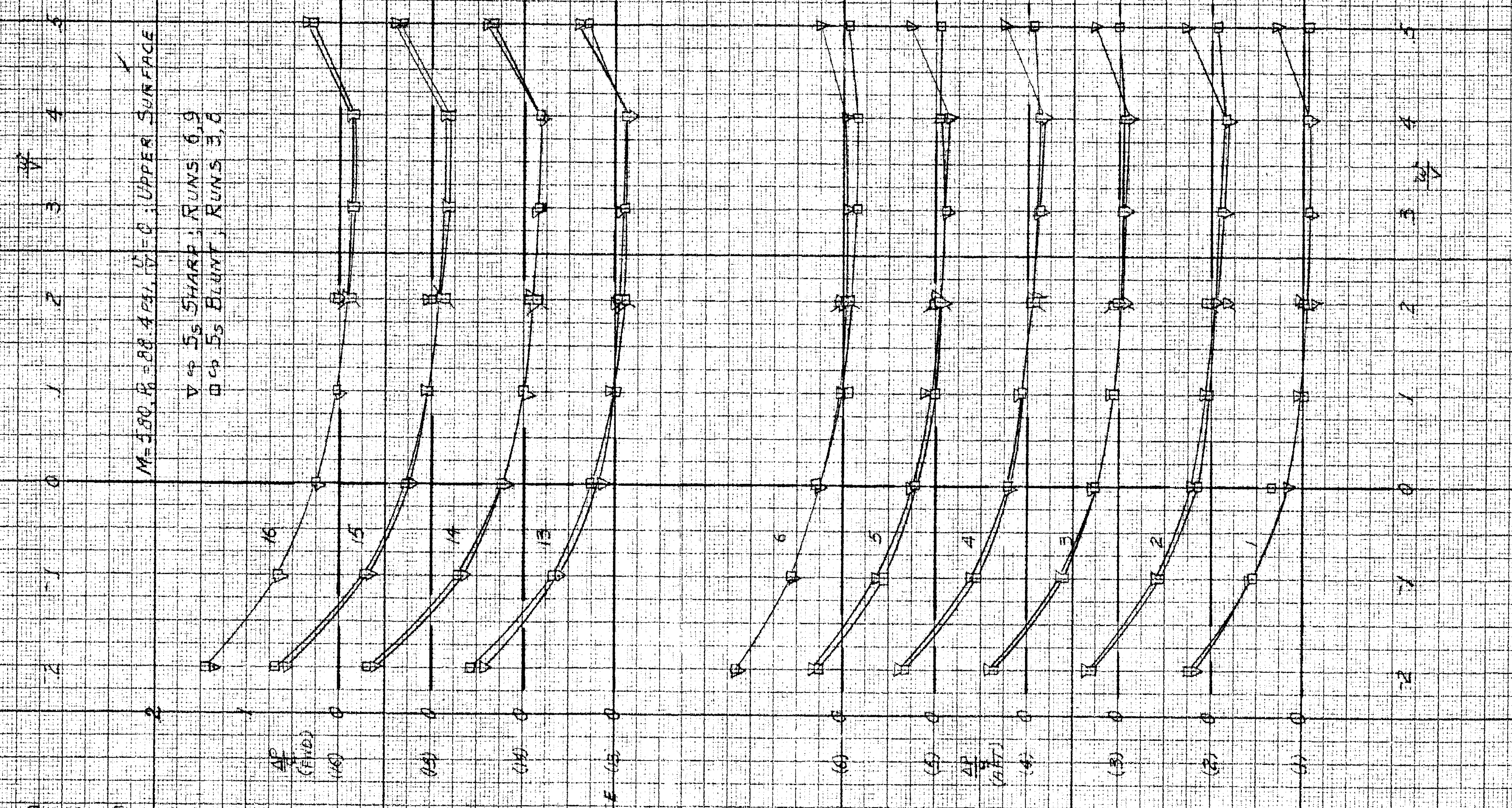

FIG. 13 EFFECTS OF BLUNTNESS, SUBSONIC EDGES,

UPPER SURFACE, $P_0 = 88.4 PSI$, $\frac{\Delta P}{q}$ VS. $\frac{w}{V}$

FIG 16 EFFECTS OF BLUNTNESS, SUPERSONIC FLOWS

UPPER SURFACE, P_o = 88 PSI, $\frac{\Delta P}{q}$ VS $\frac{x}{y}$

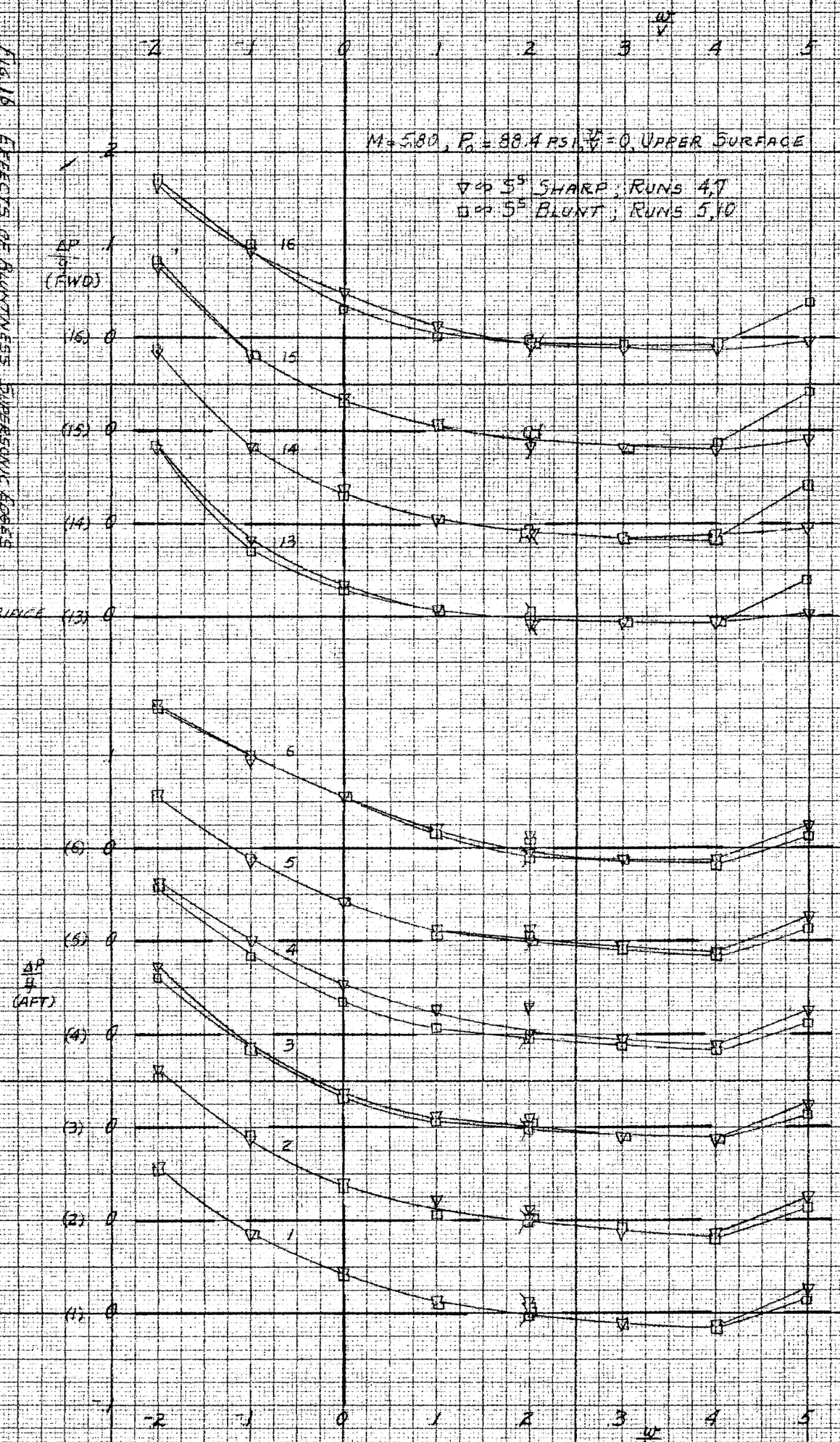

NOTE: TUBE 15 (□) PARTIALLY PLUGGED AT $\frac{x}{y}$ = 3, 4; POINTS ARE AVERAGE OF TUBES 14 AND 16

FIG. 18 EFFECTS OF BLUNTNESS IN VARIOUS SUBSONIC CODES

$M = 5.80$, $P_0 = 88.4$ PSI, $\frac{r'}{r} = 125$, $\frac{r''}{r} = 201$

Δ, ∇ ⇨ LOWER, UPPER; S_5 SHARP, RUNS 6, 9

$\circ, \square$ ⇨ " , " ; " " , RUNS 3, 8

Δ ⇨ STAGNATION (COMPUTED)

$\frac{\Delta P}{q}$ (FWD)

$\frac{\Delta P}{q}$ (AFT)

$\frac{\Delta P}{q}$ vs. $\frac{2y}{d}$

$\frac{2y}{d}$

Fig. 19 Effects of Clearances in Yaw Surface Static Probes

$M = 5.80$, $P_0 = 88.4$ psi, $\frac{w}{V} = .125$, $\frac{w}{l} = .201$

△, ▽ ⤷ Lower, Upper, 5° Sharp, Runs 4, 7

○, □ ⤷ " , " ; 5° Blunt, Runs 5, 10

◇ ⤷ Stagnation (Computed)

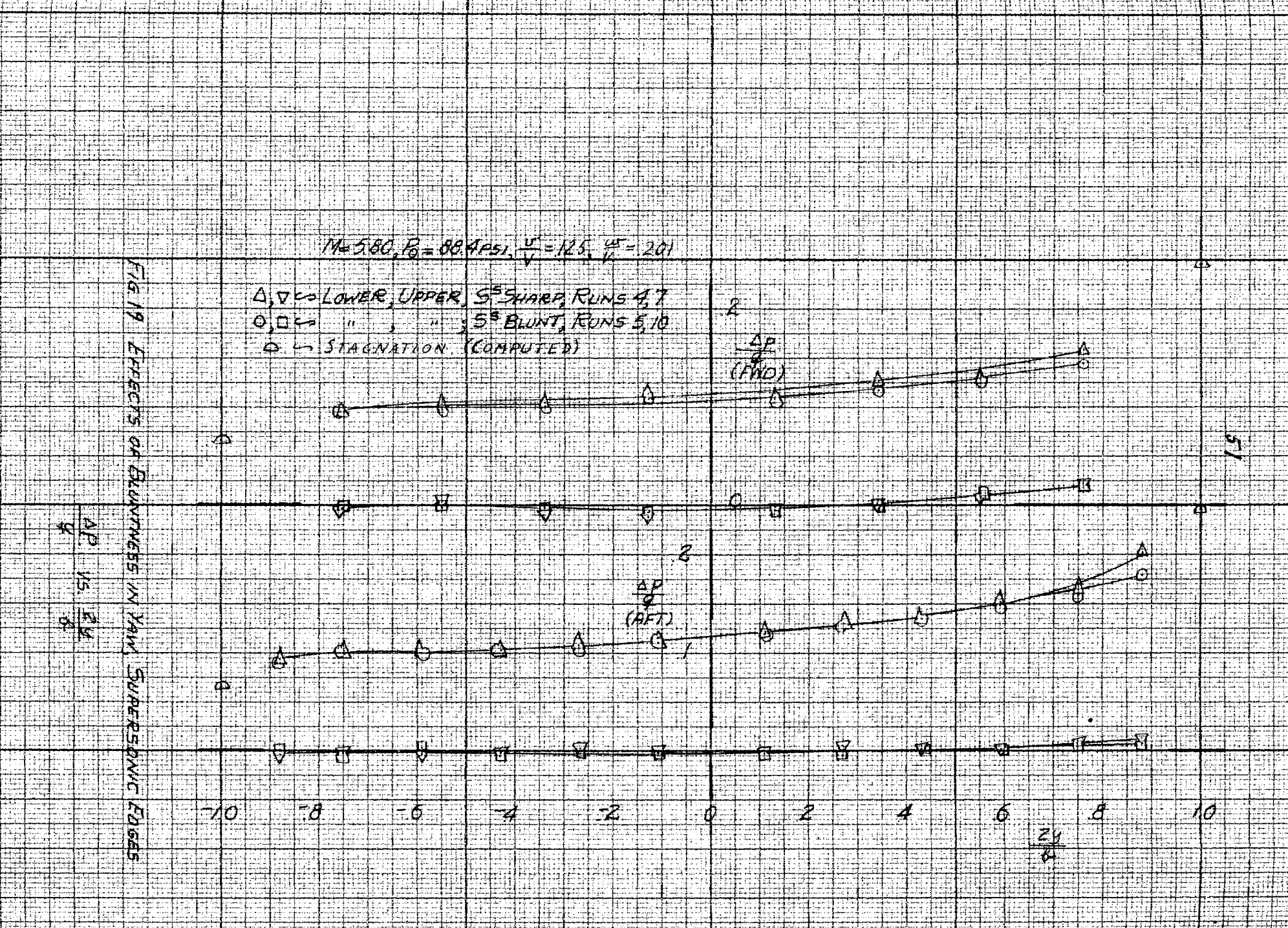

FIG. 20 EFFECTS OF BLUNTNESS, SUBSONIC EDGES
LOWER SURFACE, $P_0 = 44.5$, $\frac{\Delta P}{q}$ VS. $\frac{w}{v}$

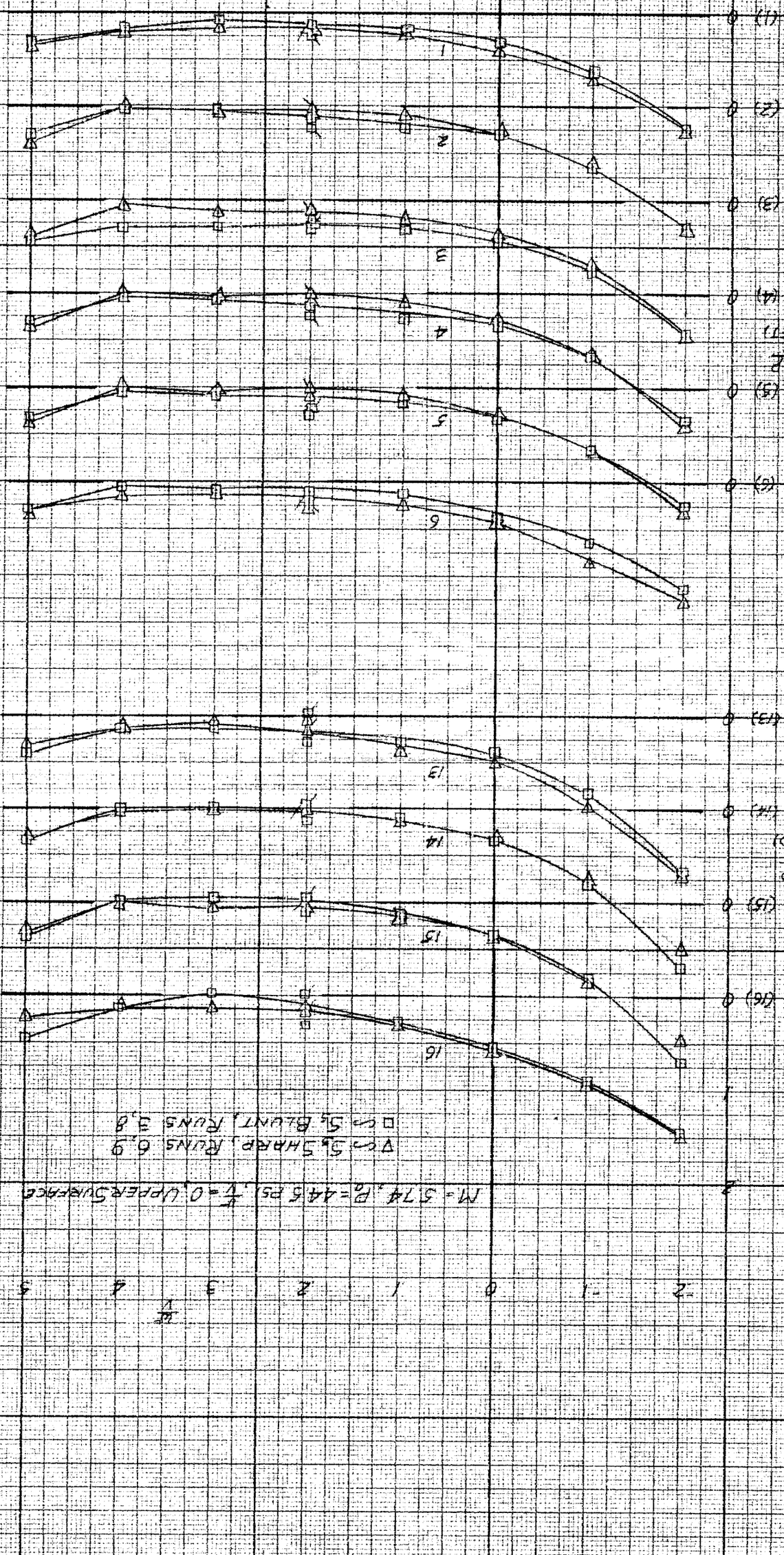

FIG. 21 EFFECTS OF BLUNTNESS, SUBSONIC EDGES
UPPER SURFACE, P_o = 44.5 PSI, $\frac{\Delta P}{q}$ VS $\frac{y}{y}$

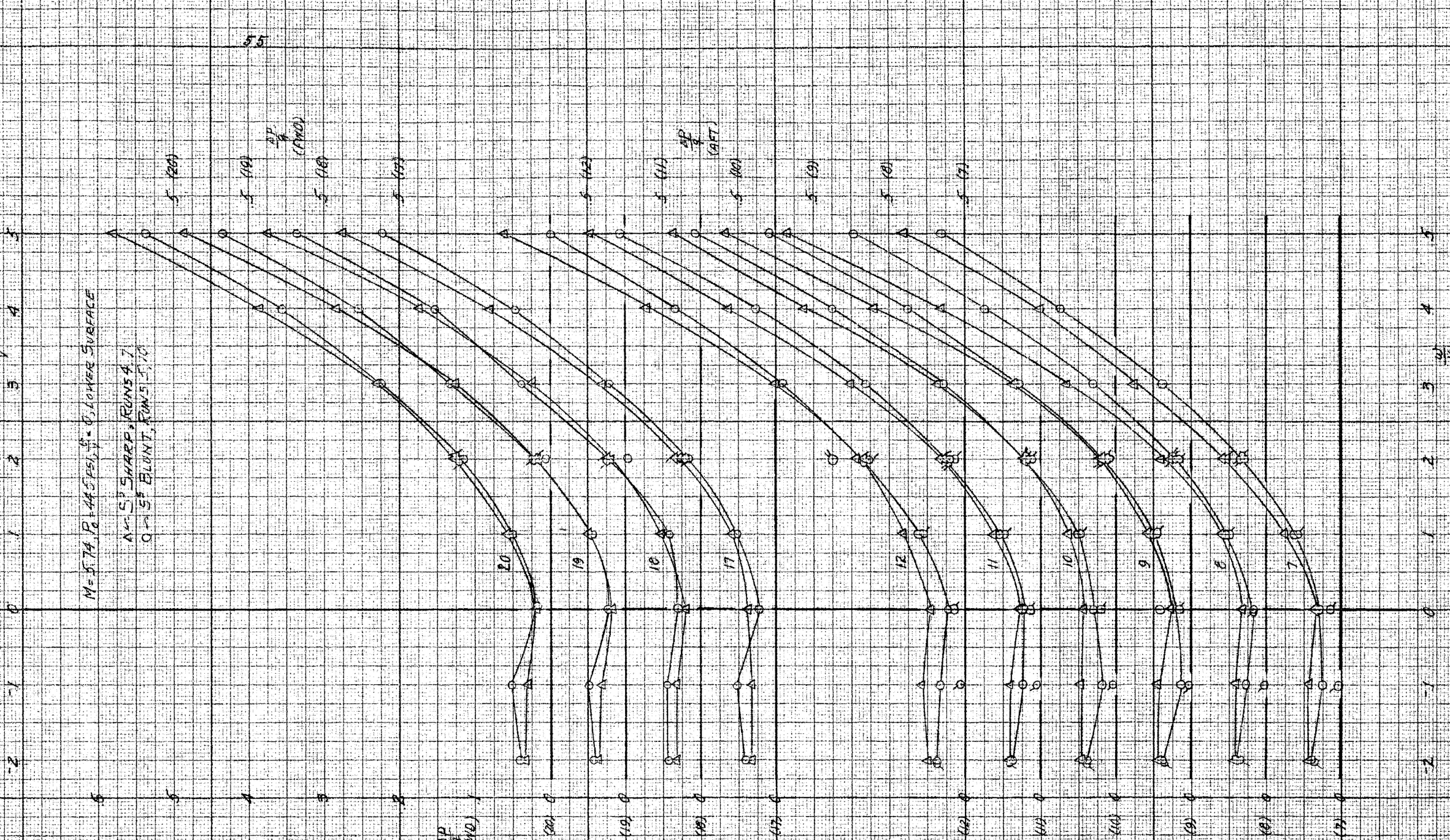

FIG 23 EFFECTS OF BLUNTNESS, SUPERSONIC EDGES

LOWER SURFACE, $P_o = 44.5$, $\frac{\Delta P}{q}$ VS $\frac{\omega}{V}$

FIG. 24 EFFECTS OF BLUNTNESS, SUPERSONIC EDGES

(UPPER SURFACE, P_0=445 PSI) $\frac{\Delta P}{q}$ VS $\frac{w}{v}$

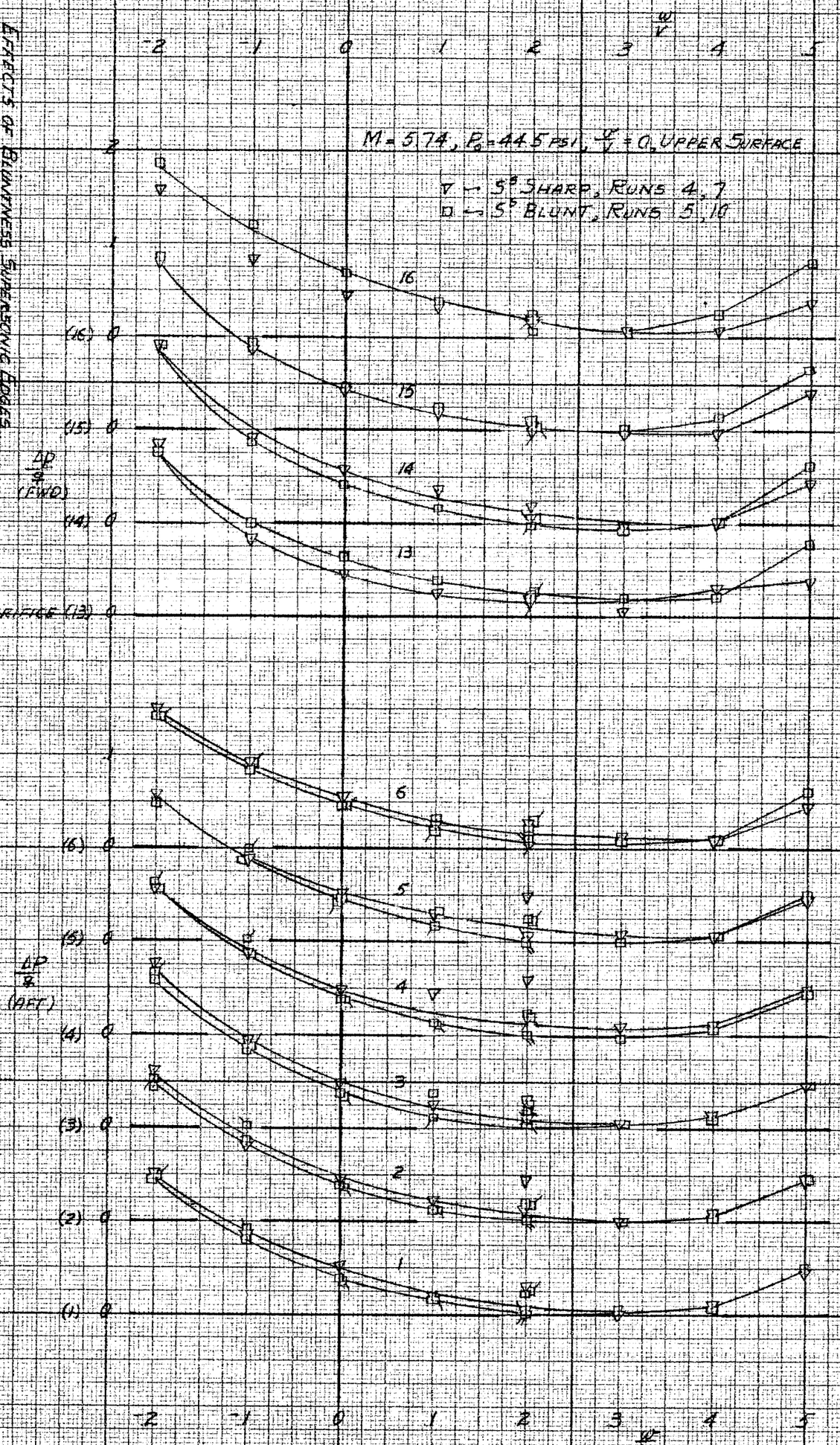

NOTES: 1. TUBE 15 (□) PARTIALLY PLUGGED FOR $\frac{w}{v} \leq -1$, POINTS PLOTTED ARE AVERAGE OF TUBES 4 AND 6

2. TUBE 16 (▽) PARTIALLY PLUGGED FOR $\frac{w}{v} \leq 0$

3. HIGH POINTS, TUBES 1-6, $\frac{w}{v} = -2$, BELIEVED TO BE EARLY SEPARATION DUE TO STRAIGHT STING

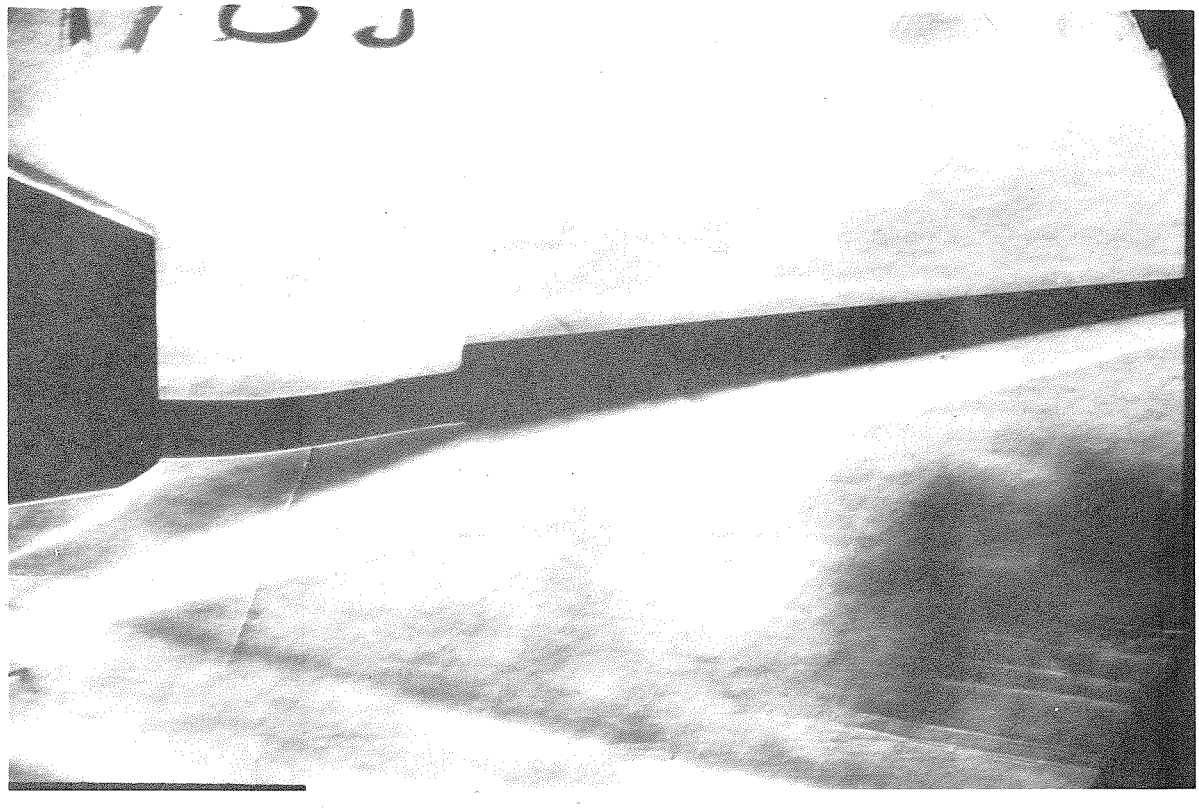

Fig. 26 Side Schlieren with tubes, subsonic sharp, w/V = .2

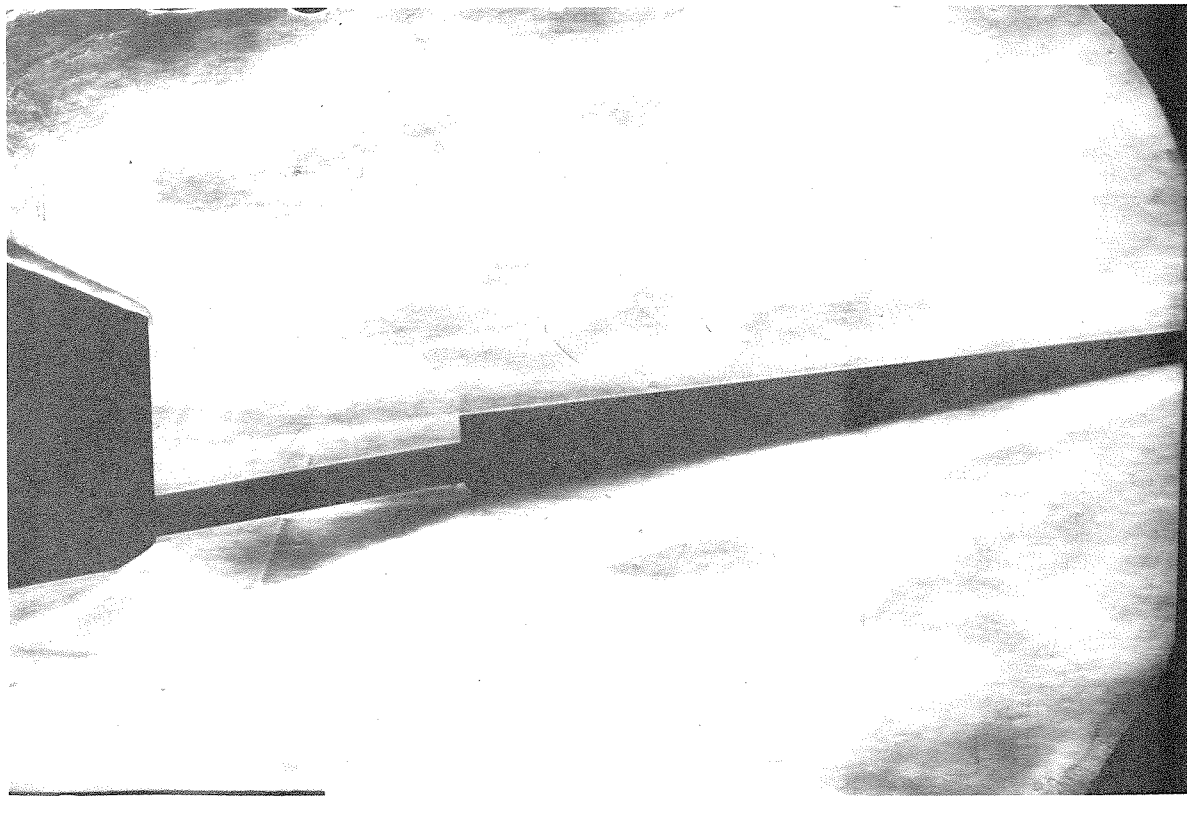

Fig. 27 Side Schlieren without tubes, subsonic sharp, w/V = .2

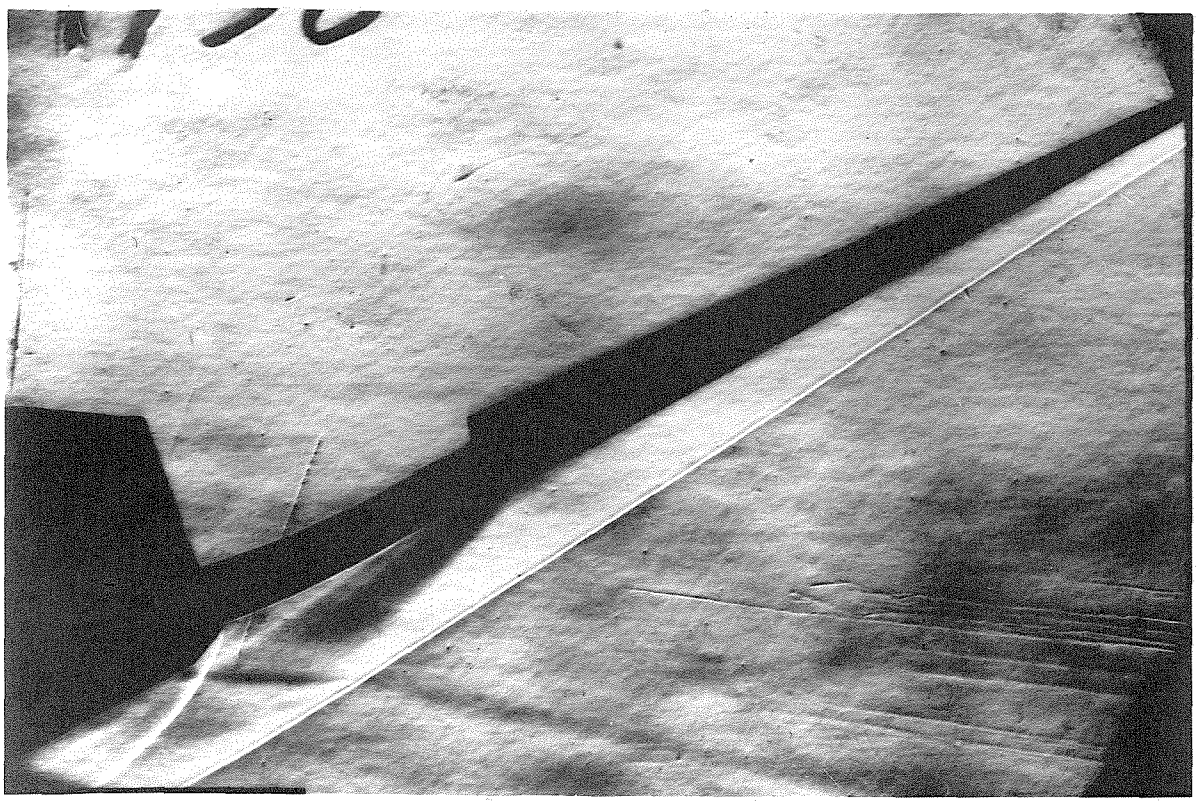

Fig.28 Side Schlieren with tubes, subsonic sharp, w/V = .5

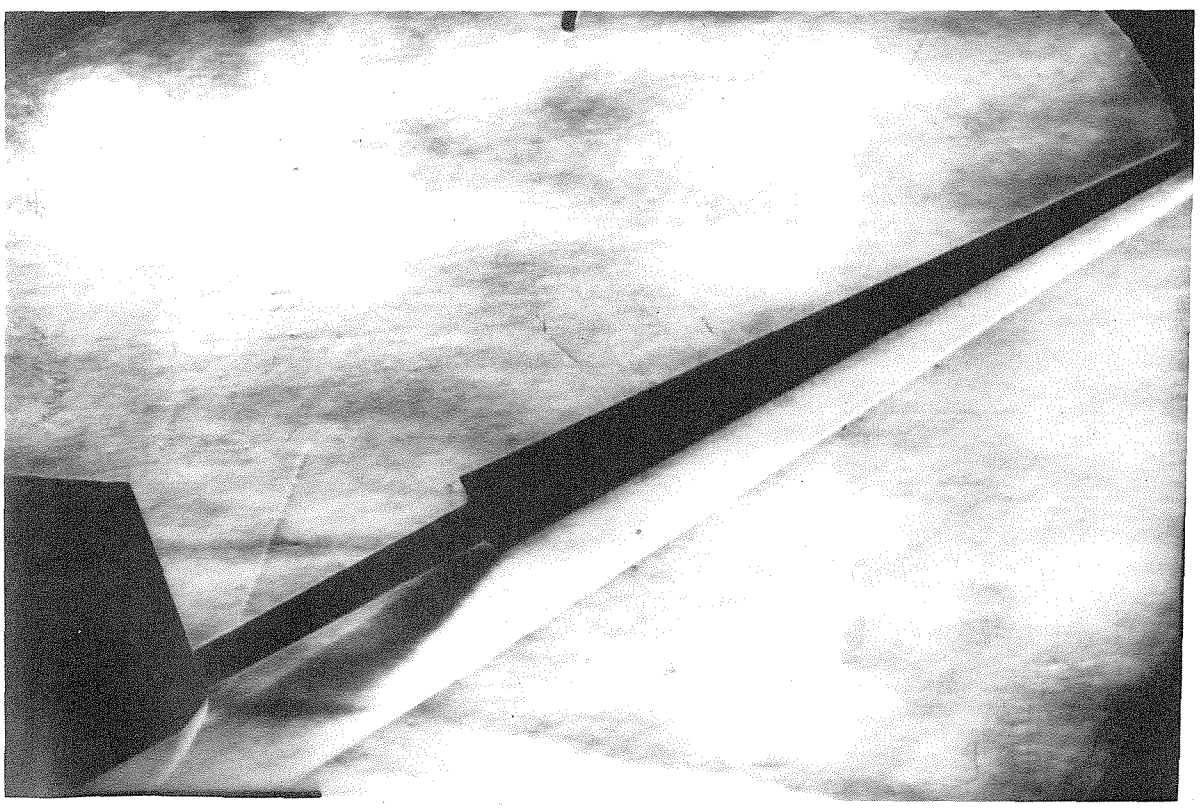

Fig. 29 Side Schlieren without tubes, subsonic sharp, w/V = .5

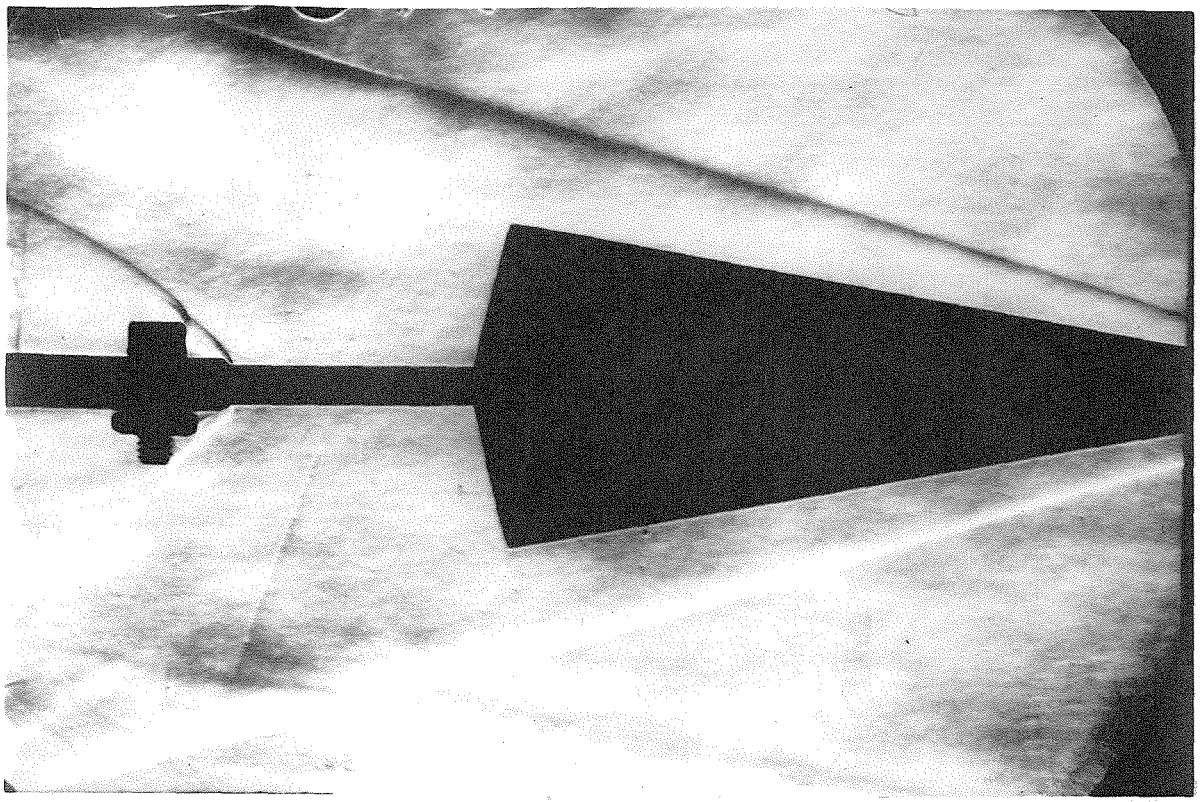

Fig. 30 Top Schlieren, subsonic sharp, w/V = .5

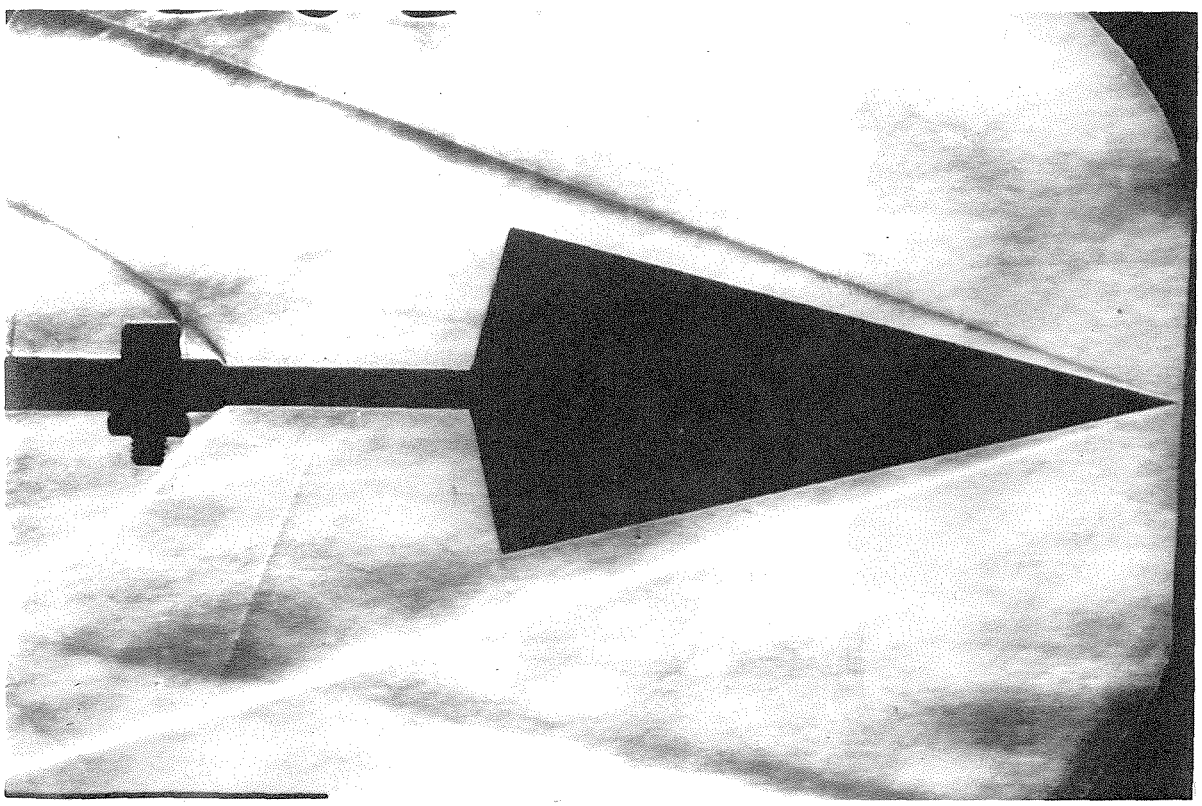

Fig. 31 Top Schlieren, supersonic sharp, w/V = .5

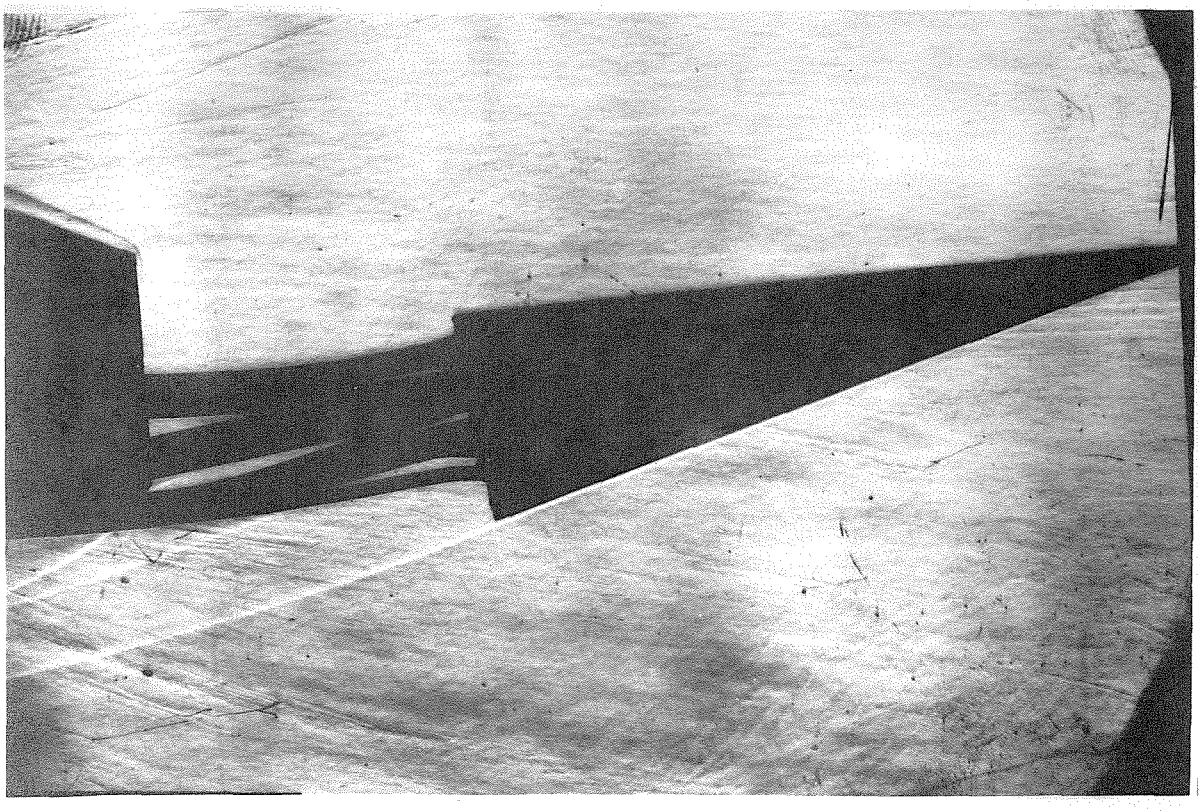

Fig. 32 Schlieren in yaw, supersonic sharp, w/V = .201, v/V = .125

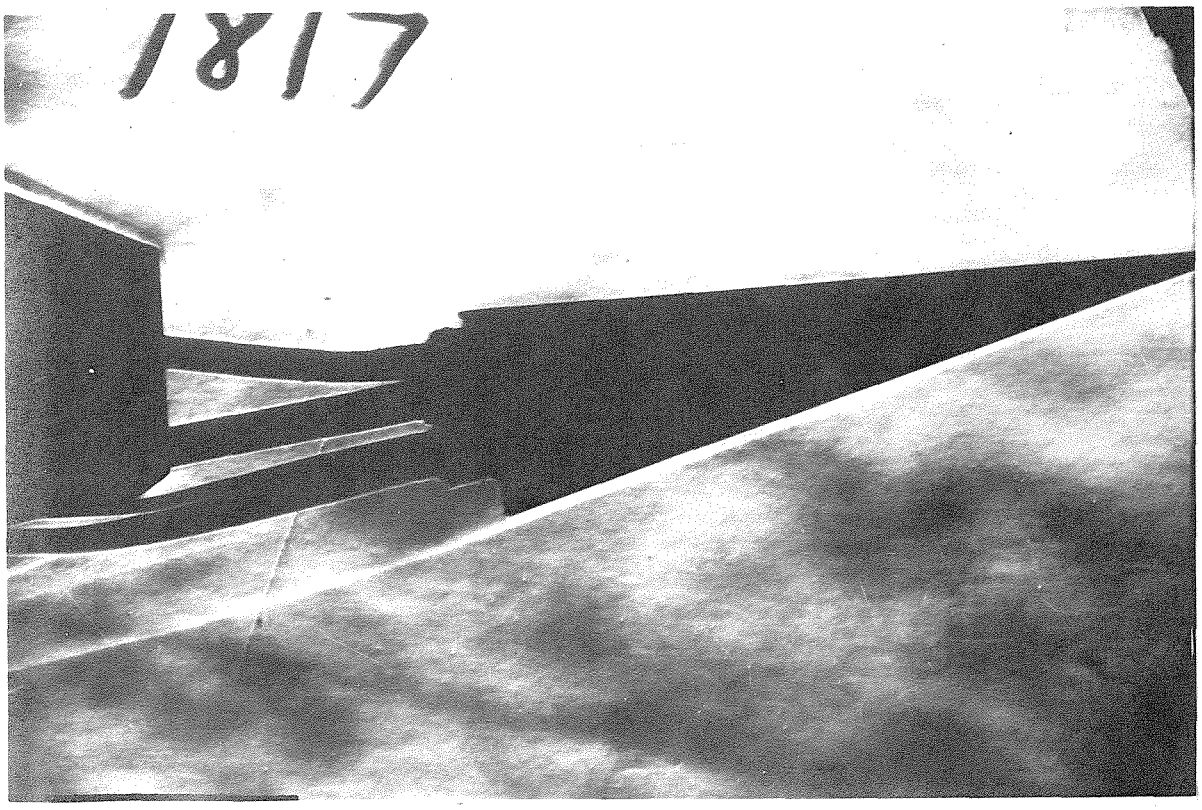

Fig. 33 Schlieren in yaw, supersonic blunt, w/V = .201, v/V = .125

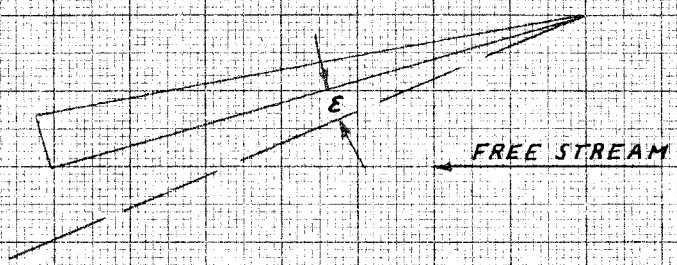

$M = 5.80$, $P_o = 88.4$ PSI, $\frac{w}{V} = 0$

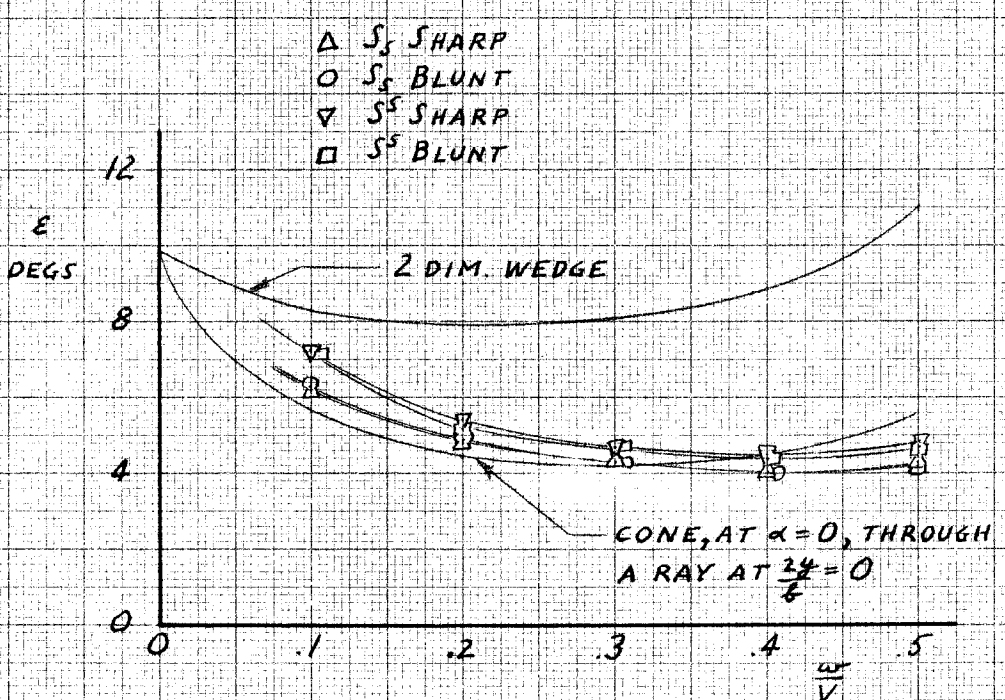

NOTE: ε IS AN AVERAGE FOR THE SHOCK SURFACE AHEAD OF THE TRAILING EDGE

FIG. 34 SHOCK SURFACE TRAVEL, SIDE VIEW DATA

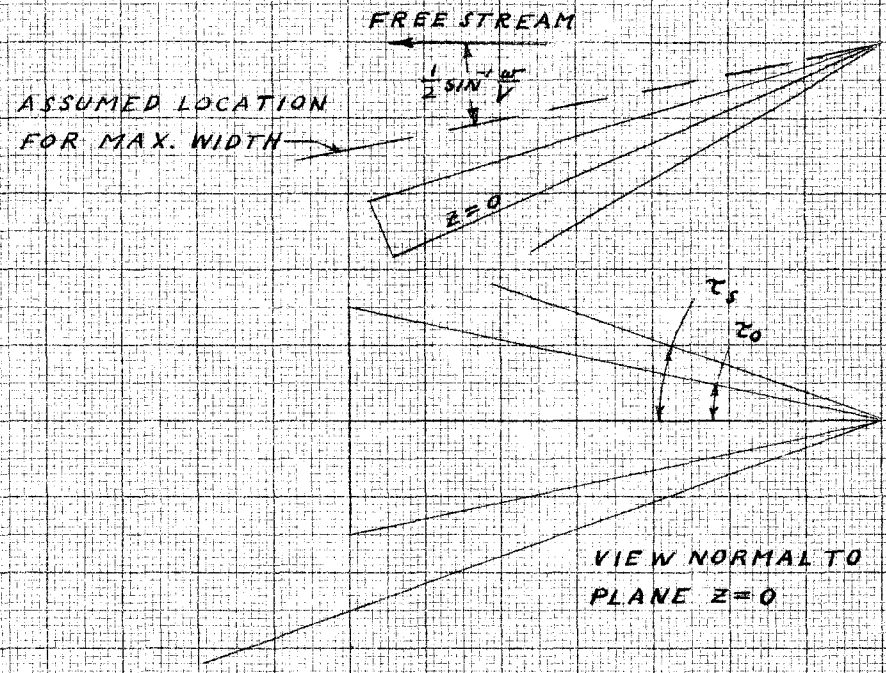

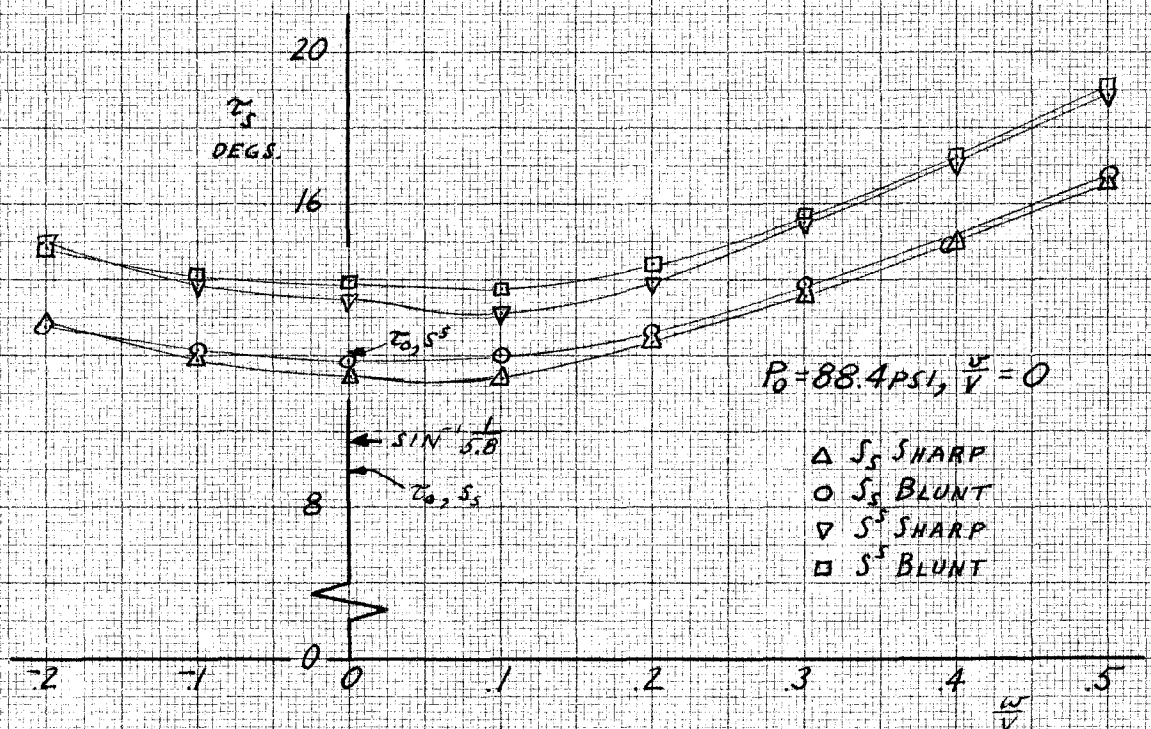

NOTE: τ_s IS AN AVERAGE FOR THE SHOCK SURFACE AHEAD OF THE TRAILING EDGE, AND INDICATES MAX. WIDTH.

FIG. 35 SHOCK SURFACE TRAVEL, TOP VIEW DATA

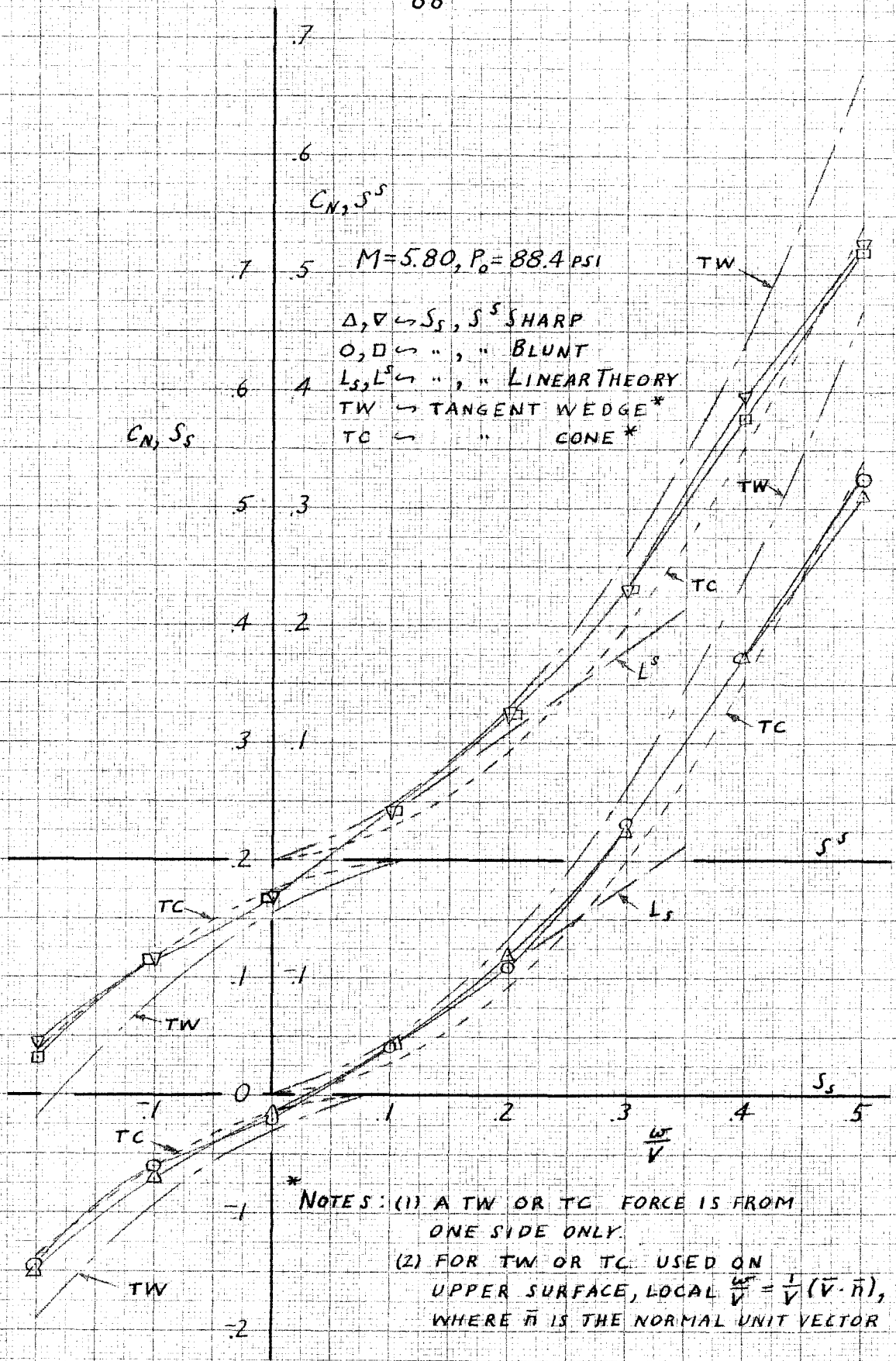

*NOTES: (1) A TW OR TC FORCE IS FROM ONE SIDE ONLY.

(2) FOR TW OR TC USED ON UPPER SURFACE, LOCAL $\frac{\omega}{V} = \frac{1}{V}(\vec{V}\cdot\vec{n})$, WHERE $\vec{n}$ IS THE NORMAL UNIT VECTOR

FIG. 38 NORMAL FORCE COMPARISONS

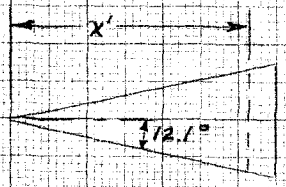

—— PRESENT REP: $\bar{X} = .253$
$M = 5.8$
$M_{n_0} = 1.215$
$x' = 3.13$ INCHES
$d \approx .001$ INCHES

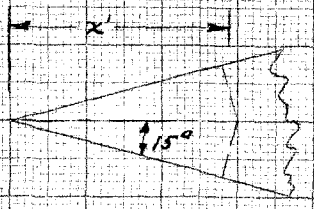

— — REFERENCE 14: $\bar{X} = 1.47$
$M = 13.3$
$M_{n_0} = 3.44$
$x' = 0.735$ INCHES
$d \approx .007$ INCHES

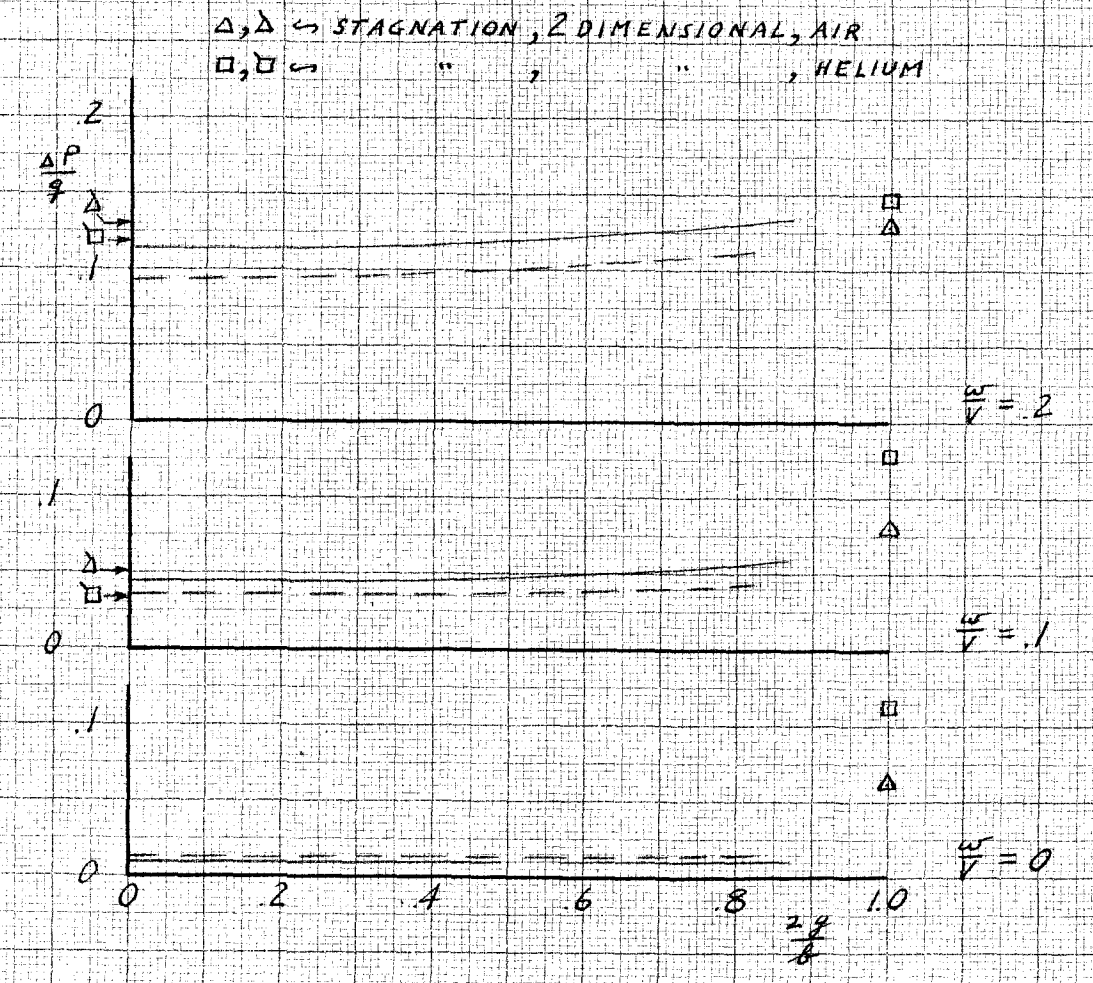

FIG. 39 COMPARISON WITH HELIUM TEST AT MACH 13.3